ELSEVIER

Journal of Structural Geology 27 (2005) 2008–2029

JOURNAL OF STRUCTURAL GEOLOGY

www.elsevier.com/locate/jsg

Granite emplacement and its relation with regional deformation in the Aravalli Mountain Belt (India)—inferences from magnetic fabric

Manish A. Mamtani[a,*], R.O. Greiling[b]

[a]*Department of Geology & Geophysics, Indian Institute of Technology, Kharagpur 721302, India*
[b]*Geologisch-Paläontologisches Institut, Ruprecht-Karls-Universität Heidelberg, INF-234, D-69120 Heidelberg, Germany*

Received 26 July 2004; received in revised form 6 June 2005; accepted 8 June 2005
Available online 9 August 2005

Abstract

This contribution presents field, microstructural and anisotropy of magnetic susceptibility (AMS) data from the Godhra Granite, a ca. 1 Ga pluton at the southern margin of the Aravalli Mountain Belt (western India) that lies near the Central Indian Tectonic Zone (CITZ). The northern and southern margins of the granite are high strain zones with north dipping, E–W striking foliations, and NW plunging stretching lineations. The presence of preferentially oriented feldspars suggests that the granite was subjected to magmatic deformation during its emplacement. High temperature solid-state deformation fabrics are recorded from microstructural studies, which imply that the granite is deformed. AMS data show magnetic foliations and magnetic lineations in the granite with orientations similar to the field data. The magnetic foliation in the granite is parallel to the D_3 foliation in the gneissic host-rock. Both the stretching lineations and the magnetic lineations at the granite margin high strain zones are parallel with the axes of D_3 reclined folds in the gneiss. Therefore, the emplacement of the Godhra Granite is inferred to have taken place syntectonically, while the gneiss was undergoing the D_3 phase of deformation. The orientation and character of these lineations and the vergence of the D_3 folds imply oblique simple shear, which is inferred to have controlled the emplacement of the granite. The magnetic fabric data are compared with the regional structural trends of the metasedimentary rocks of the southern Aravalli region and the available geochronological data from rocks of the southern Aravalli region are summarised. Based on this information, it is suggested that the emplacement of Godhra Granite, deformation of the southern parts of Aravalli Mountain Belt and, tectonothermal events along the CITZ and Rodinia Supercontinent assembly were related events.

Keywords: Anisotropy of magnetic susceptibility; Granite emplacement; High-strain zone; Microstructure; Aravalli Mountain Belt; Rodinia Supercontinent; India

1. Introduction

Recent research on granitic rocks reveals that crustal anatexis, granite melt extraction, ascent, emplacement and crustal deformation may be interrelated and synchronous processes (Solar et al., 1998; Pressley and Brown, 1999). In many convergent orogenic belts, spatial and temporal relationships between granite and regional tectonic structures suggest ascent and emplacement during contraction rather than during extension (Hutton, 1997; Brown and Solar, 1998a). Moreover, a close relationship has been established between granitic plutons, shear zone systems and transpressive convergent zones (D'Lemos et al., 1992; Ingram and Hutton, 1994; Leblanc et al., 1996; Brown and Solar, 1998a,b; Pressley and Brown, 1999; Greiling and Verma, 2001). However, correlating granite emplacement and deformation with regional tectonic events is a challenge because granitic rocks do not always develop mesoscopic scale deformation fabrics. Microstructural studies of granites can help to identify magmatic or solid-state deformation fabrics (e.g. Simpson, 1985; Paterson et al., 1989; Bouchez et al., 1990), on the basis of which granite can be interpreted as deformed. In itself, this cannot lead to infer the relationship between a regional deformation event and development of a fabric in granite. Additional information is required, in particular on the orientation and spatial distribution of these fabrics and their relationship with host rocks of the granite pluton in question. Anisotropy

* Corresponding author. Tel.: +91 3222 283388; fax: +91 3222 255303/282700
E-mail address: mamtani@gg.iitkgp.ernet.in (M.A. Mamtani).

0191-8141/$ - see front matter © 2005 Elsevier Ltd. All rights reserved.
doi:10.1016/j.jsg.2005.06.004

of magnetic susceptibility (AMS) studies are used to produce this additional data on the relationship between granite intrusion, fabric development and regional tectonics (e.g. Archanjo et al., 1994; Cruden and Launeau, 1994; Rochette et al., 1994; Scaillet et al., 1995; Bouchez, 1997; Benn et al., 1998, 1999, 2001; Pignotta and Benn, 1999; Siegesmund and Becker, 2000; de Wall et al., 2001; Greiling and Verma, 2001; Ferré et al., 2002; Neves et al., 2003; Tomezzoli et al., 2003; Gattacceca et al., 2004).

The southern part of the Aravalli Mountain Belt (AMB), western India has a granite pluton referred to as the Godhra Granite. The relationship between emplacement of this granite and regional tectonics has so far remained unexplored. From a global perspective, this region is important because the Godhra Granite has proximity to the Son-Narmada North Fault (SNNF) that is commonly referred to as the Narmada-Son lineament (Fig. 1a), which along with the Godavari lineament is believed to have formed during the growth of the Indian shield in Mesoproterozoic times; the latter is envisaged to have formed due to accretion of the Aravalli, Dharwar and Singhbhum Protocontinents (Naqvi et al., 1974). According to Yedekar et al. (1990), the suturing of the northern and southern Indian shields took place along the Central Indian Tectonic Zone (CITZ) during the Paleoproterozoic period (ca. 2200–2100 Ma) and the SNNF is the northern extremity of the CITZ. The latter is also known to have rejuvenated and experienced subsequent tectonothermal events during the Grenvillian period (Yoshida et al., 2001; Bhowmik and Dasgupta, 2004), which is also the time when the Rodinia Supercontinent assembly took place (Condie, 2001). To the north of the CITZ lies the Bundelkhand craton (Fig. 1c) and to the south lies the Bastar craton. The western extension of the CITZ is regarded to continue to the Aravalli–Delhi fold belt, which runs along the western fringe of the Bundelkhand block (Fig. 1c). There is evidence of some granitic activity during the Grenvillian period ($\sim$1 Ga) in the northern parts of the AMB, e.g. the Sendra Granitoid Suite (Tobisch et al., 1994; Pandit et al., 2003) and the Ambaji granite (Crawford, 1975). The Godhra Granite is also of a similar age and because of its spatial proximity to the CITZ, it is important to understand whether the accretionary tectonic events along the CITZ, deformation of the southern parts of AMB and emplacement of the Godhra Granite are related events. With the aim of deciphering the above, in this paper we present field, microstructural and AMS data from the Godhra Granite and its country rock (banded gneiss).

2. Regional geology

The Godhra Granite dated at 955 ± 20 Ma by whole rock Rb–Sr method (Gopalan et al., 1979) occupies an area of about 5000 km^2 in the southern parts of the AMB. The latter is a major Precambrian mountain belt of India that extends $\approx$700 km from the south of Delhi to the western parts of India. An assemblage of gneiss–granite–amphibolite forms the Archaean basement of the AMB (Heron, 1953; Gopalan et al., 1990; Wiedenbeck et al., 1994; Roy and Kröner, 1996). This complex forms the basement for the Aravalli and Delhi metasedimentary supergroups. Both supergroups have undergone polyphase deformation and inversion tectonics during Palaeoproterozoic and Mesoproterozoic times (e.g. Verma and Greiling, 1995).

To the north and south of the Godhra Granite, metasedimentary rocks of the Aravalli Supergroup outcrop. In the south, the granite is also in contact with a banded gneiss unit (Fig. 1b). Field relationships indicate that the gneiss is older than the granite (Mamtani et al., 2002). To the north and east, the granite is in contact with quartzite and schists of the Lunavada Group, a unit of the Aravalli Supergroup (Gupta et al., 1995). These metasediments have undergone three deformation events (D_1–D_3) associated with regional metamorphism and exhumation (Mamtani et al., 1999a,b, 2000, 2001; Bakker and Mamtani, 2000). D_1 and D_2 resulted in development of coaxial folds with SW striking axial planes and formation of Type-III interference patterns. D_3 resulted in folds with NW to W striking axial surfaces. The superposition of D_3 over D_1/D_2 folds resulted in Type-I interference patterns. To the southwest, the granite is in contact with the Champaner Group, which comprises low-grade phyllites and quartzites and stratigraphically overlies the Lunavada Group (Fig. 1). It is known to have a simple deformation history involving only one major deformation event that resulted in folds with WNW to W striking axial planes (Jambusaria and Merh, 1967; Gopinath et al., 1977).

In order to determine the time relationship between fabric development in the granite and deformation in the gneiss a 900 km^2 area has been investigated around the towns of Devgadh Bariya and Sagtala (Fig. 1), where the contacts between the granite, the gneiss and the Lunavada metasedimentary rocks are exposed.

3. Structures in banded gneiss

The banded gneiss in the study area is migmatitic and comprises biotite-rich layers alternating with layers of quartzo-feldspathic leucosomes. Mineralogically, it is composed of quartz, K-feldspar, plagioclase and biotite, and in places, amphibolite bands are also present. Although the rocks dominantly show a single banding or foliation in the field, detailed fieldwork and structural analysis reveal that this banding is a transposed structure that preserves evidence of several deformations.

A deformation history comprising three episodes of deformation D_1, D_2 and D_3 has been worked out. Evidence of D_1 in the form of folds is rare in the study area and folds related to D_2 are also scarce. Wherever observed, they fold the pre-existing foliation (S_1) inferred to have developed

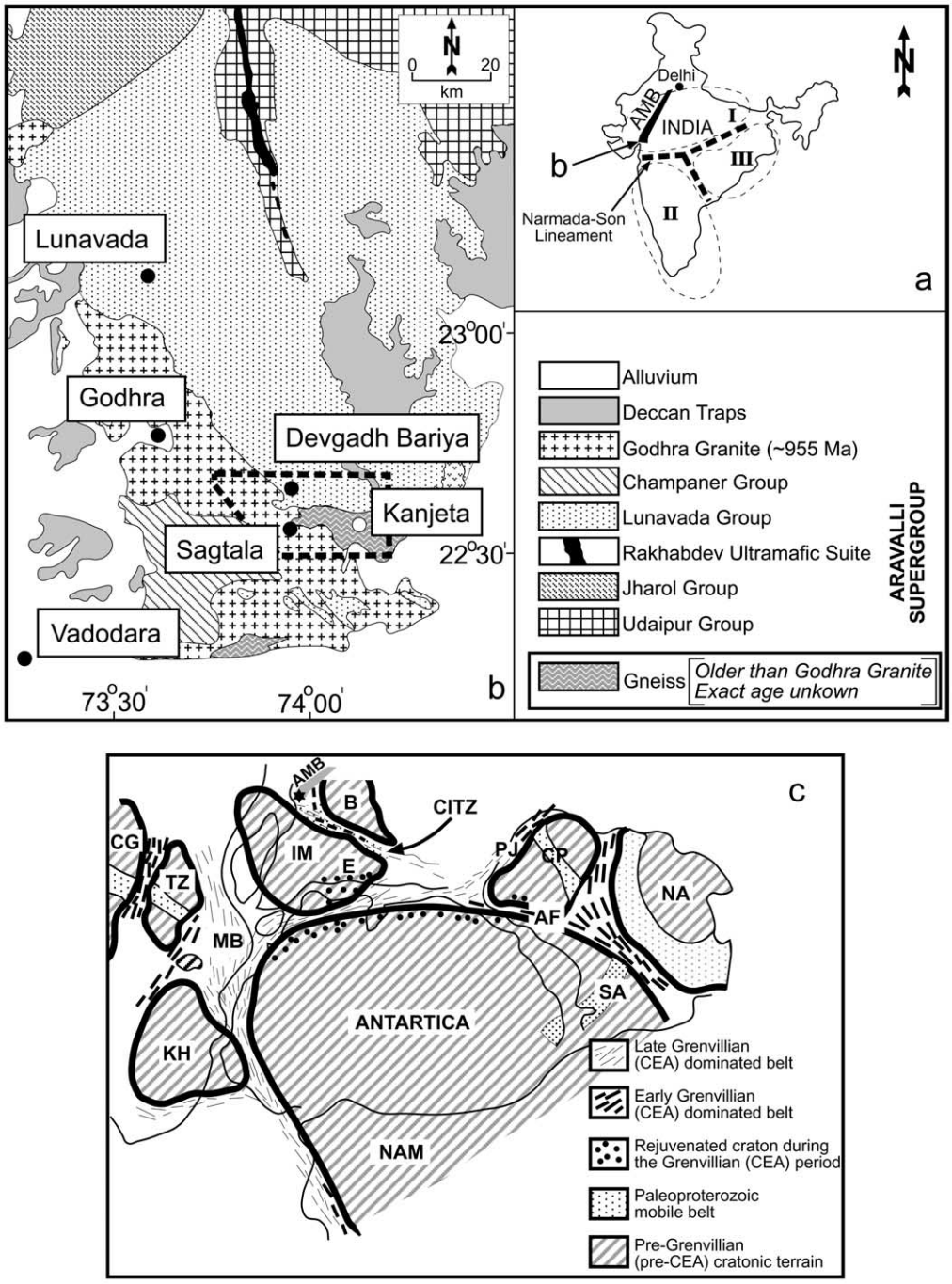

Fig. 1. Location of the study area. (a) General location map. Areas marked I, II and III are the Aravalli, Dharwar and Singhbhum protocontinents, believed to have accreted during Mesoproterozoic times to form the Indian shield (after Naqvi et al., 1974). The accretion took place along the Y-shaped Narmada-Son-Godavari lineament. (b) Lithostratigraphic map of the south Aravalli Mountain Belt (AMB), western India (modified after maps of Geological Survey of India, Gupta et al., 1995). Boxed region is the study area detailed in Fig. 4. (c) Position of Aravalli Mountain Belt (AMB; shown in grey shade in the top part of the figure) and the Godhra Granite (shown by star) during the Grenvillian period when amalgamation of east Gondwana took place (modified after Yoshida et al., 2001). AF, Albany Fraser orogen; B, Bundelkhand block; CEA, Circum East Antartic; CG, Congo craton; CP, Capricon orogen; CITZ, Central Indian Tectonic Zone; IM, India Madagascar paleocontinent, including Bastar craton; E, Eastern Ghats Belt; KH, Kalahari craton; NA, North Australian craton; MB, Mozambique Belt; NAM, North American craton; PJ, Pinjarra orogen; SA, South Australian craton.

axial planar to D_1 folds. These D_1 folds and associated planar structures were refolded due to tight isoclinal D_2 folding. The D_2 folds are tight and inclined with SW to WSW striking axial surfaces (S_2) that dip moderately to the northwest. The presence of a hook-shaped geometry due to the refolding of D_1 folds (Type-III interference pattern) is observed at Dudhiya (Fig. 2a; see Fig. 4 for location). As a result, evidence of D_1 folds has been mostly obliterated.

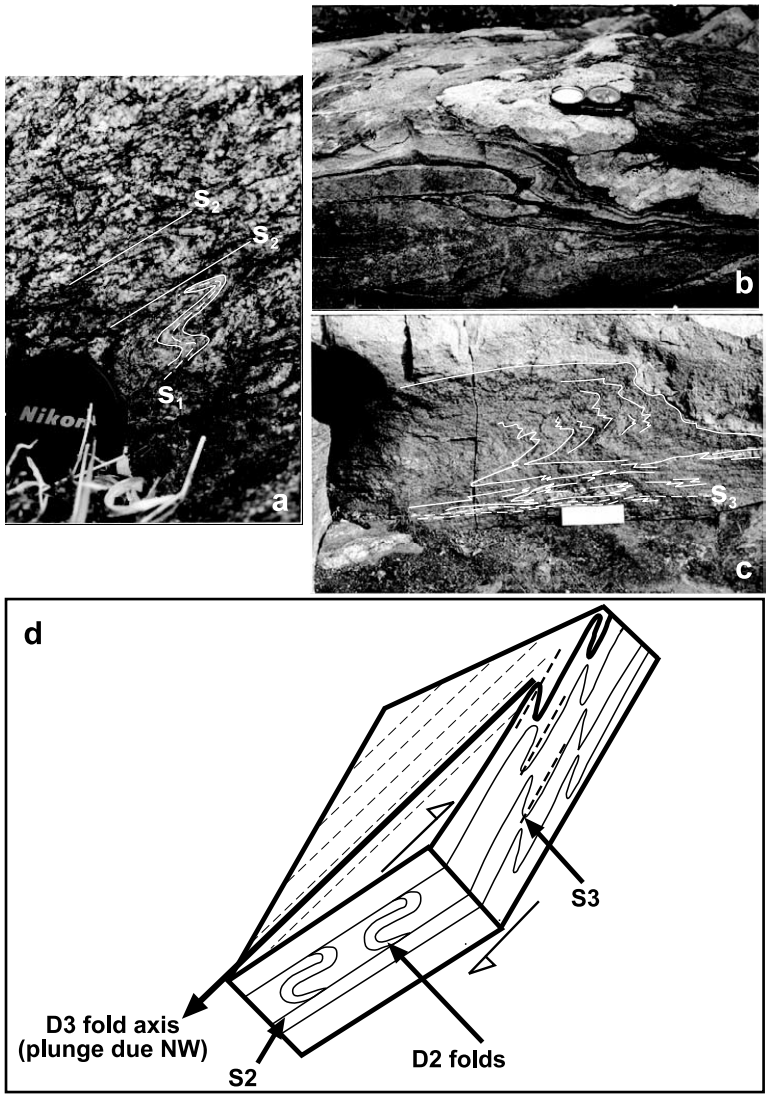

Fig. 2. Mesoscopic structures in banded gneiss. (a) D_2 folds in banded gneiss folding a S_1 foliation (dashed) that developed during an earlier D_1 folding. The gneissic layering (S_0) is refolded thus giving a Type-3 interference pattern. (b) D_3 folds in banded gneiss showing a reclined geometry and folding S_2. The fold axis plunges towards the NW. (c) Ductile shearing on S_2 during D_3 folding. (d) Schematic line drawing showing the formation of D_3 reclined folds due to shearing on S_2 foliation. Note, S_2 and axial plane of D_3 folds (S_3) have similar orientation except at the hinges of D_3 folds.

Strongly verging, asymmetric folds produced during subsequent deformational phase, D_3, overprint S_2. The mesoscopic folds observed in the area dominantly belong to the D_3 event. In the vicinity of Devgadh Bariya, the D_3 folds have a reclined geometry with axial surfaces and axial plane foliation (S_3) having a strike that varies between WNW and WSW with moderate to steep northerly dip (Fig. 2b); at places vertical dips are also recorded. Since S_2 was folded to form D_3 reclined folds, S_2 is also vertical at the hinge parts of reclined folds. Evidence of ductile shearing on S_2 during D_3 is observed at several localities (Fig. 2c). D_3 reclined folds are inferred to have developed during the shearing (Fig. 2d). Note that the axial surfaces of D_2 and D_3 folds have similar orientation (Fig. 3a). The pole diagram of S_3 (Fig. 3b) from different parts of the study area show that the strike of S_3 foliation dominantly ranges between WNW and WSW. The calculated intersection axis (π-axis; Fig. 3b) plunges to the NW, to the same direction as the D_3 fold axis lineations recorded in the field (Fig. 3a).

Fig. 4 is the structural map of the study area, in the vicinity of Devgadh Bariya, where the Godhra Granite is in contact with the Lunavada Group in the north and the gneiss in the south. These contacts are observed to be high strain zones where ductile shearing and mylonitization took place. Sheared rocks were also noted at other localities in the gneiss (dashed lines in Fig. 4).

4. Structures in the Godhra Granite and its margin

The Godhra Granite is dominantly porphyritic in nature, although fine-grained varieties are noted at places, with

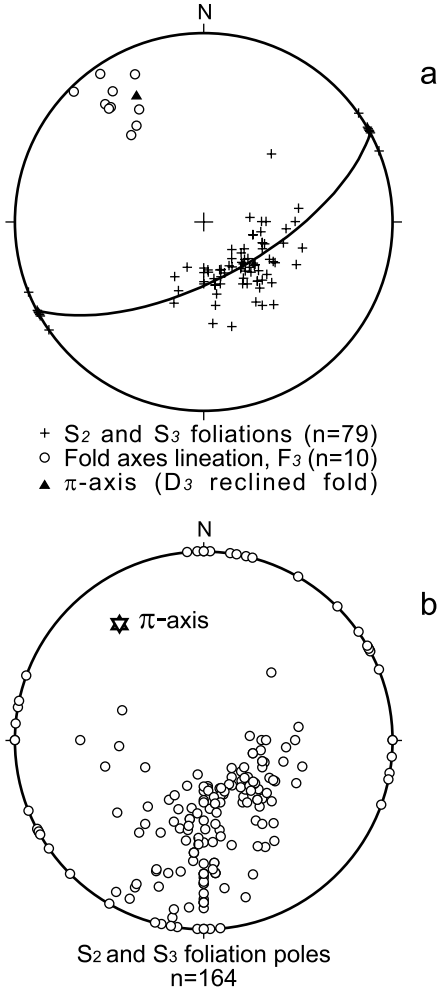

Fig. 3. Structural analyses of planar and linear structures in banded gneiss. (a) Lower hemisphere equal area projection of field data related to D_3 reclined folds observed in the vicinity of Singor/Dudhiya. (b) Synoptic π-diagram of S_3 foliation data collected from the entire study area. Note that the D_3 fold axes (π-axis) plunge towards the NW.

quartz, K-feldspar, plagioclase and biotite as the dominant minerals. In the area of investigation, the foliation at the northern margin of the granite strikes close to E–W, parallel to the margin, and dips moderately to the north, and mylonites with the same orientation are also recorded at Gadha (Fig. 4). A strong stretching lineation plunging to the northwest developed in these mylonites. The XZ section (i.e. parallel to the lineation and perpendicular to the foliation) shows S–C fabric (Berthé et al., 1979), mica fish (Lister and Snoke, 1984) (Fig. 5a) and asymmetric quartz strain shadows around feldspar porphyroclasts (Fig. 5b). These microstructures indicate a dextral sense of shear. In the geographic reference frame, this gives a top-to-the-southeast sense of shear.

At its contact with the gneiss, a complex succession of deformational fabrics is observed in the gneiss. A south–north traverse across the contact zone near Ankli (Fig. 4) reveals an increase in intensity of field fabric from within the gneiss towards the contact with the granite, which points to the presence of a high strain zone at the contact. Asymmetric folds similar to those in Fig. 2b are present in the gneiss. Towards the northern margin of this area, these folds become flattened, giving the rocks a banded appearance, with the foliation or banding striking E–W and dipping to the north (Fig. 6a). Further north, close to the contact, the bands pinch out, and eventually disappear (Fig. 6b). Here, the gneissic foliation strikes similar to that mentioned above and contains a mineral lineation plunging moderately to the NW. The adjacent contact zone in the granite shows a gneissic foliation with the same orientation. This deformation, evidenced at the margin of the Godhra Granite, is also present in the granite at some distance away from the high-strain margin, in the form of a W- to WNW-trending foliation defined by parallel alignment of feldspar laths and biotite crystals (Fig. 6c). In areas very remote from the contact, the granite does not contain a foliation visible in the field, although at some places feldspars are preferentially aligned as mentioned above.

At the microscopic scale, the studied granite samples, including those that lie away from the granite margin, show solid-state deformation microstructures. The quartz crystals have strong undulatory extinction attesting to intracrystalline deformation. Samples close to the northern margin of the granite show chess-board texture in quartz (Fig. 7a), in which square subgrains with boundaries parallel to both prism and basal planes attest to deformation at high-temperature (e.g. Blenkinsop, 2000). Quartz crystals with serrated grain boundaries implying grain boundary migration recrystallization (Passchier and Trouw, 1996) are common. Deformation twins in feldspar (Fig. 7b) and kinked biotites are noted. Myrmekite (Fig. 7c), which has been inferred as a deformation induced texture (Simpson and Wintsch, 1989) and microcline twinning in K-feldspar (Vernon, 2000) are also present in the granite margin. Besides, ductilely deformed feldspar and recrystallized feldspar are also observed (Fig. 7d). All the above microstructures imply that the margin of the granite developed intense deformation in the solid-state and at rather high temperatures. Feldspars are known to undergo deformation and recrystallization above 450–500 °C (Simpson, 1985; McCaffrey et al., 1999) and their presence in the studied rocks suggests that their deformation took place above 450 °C. It may have been well above 450 °C, as basal sub-boundaries (chess-board subgrains) of Mainprice et al. (1986) in quartz are present.

The field fabric in the granite becomes weaker in areas away from the margin. At the microscopic scale the granites have euhedral feldspars with very prominent growth twins and zoning (Fig. 7e) indicating that they were originally igneous phenocryts. Fractured feldspars whose fractures are filled up with quartz (Fig. 7f) provide evidence of submagmatic solid-state deformation (McCaffrey et al., 1999). Besides this, evidence of high-T solid-state fabric is also present in such samples. This indicates that a magmatic

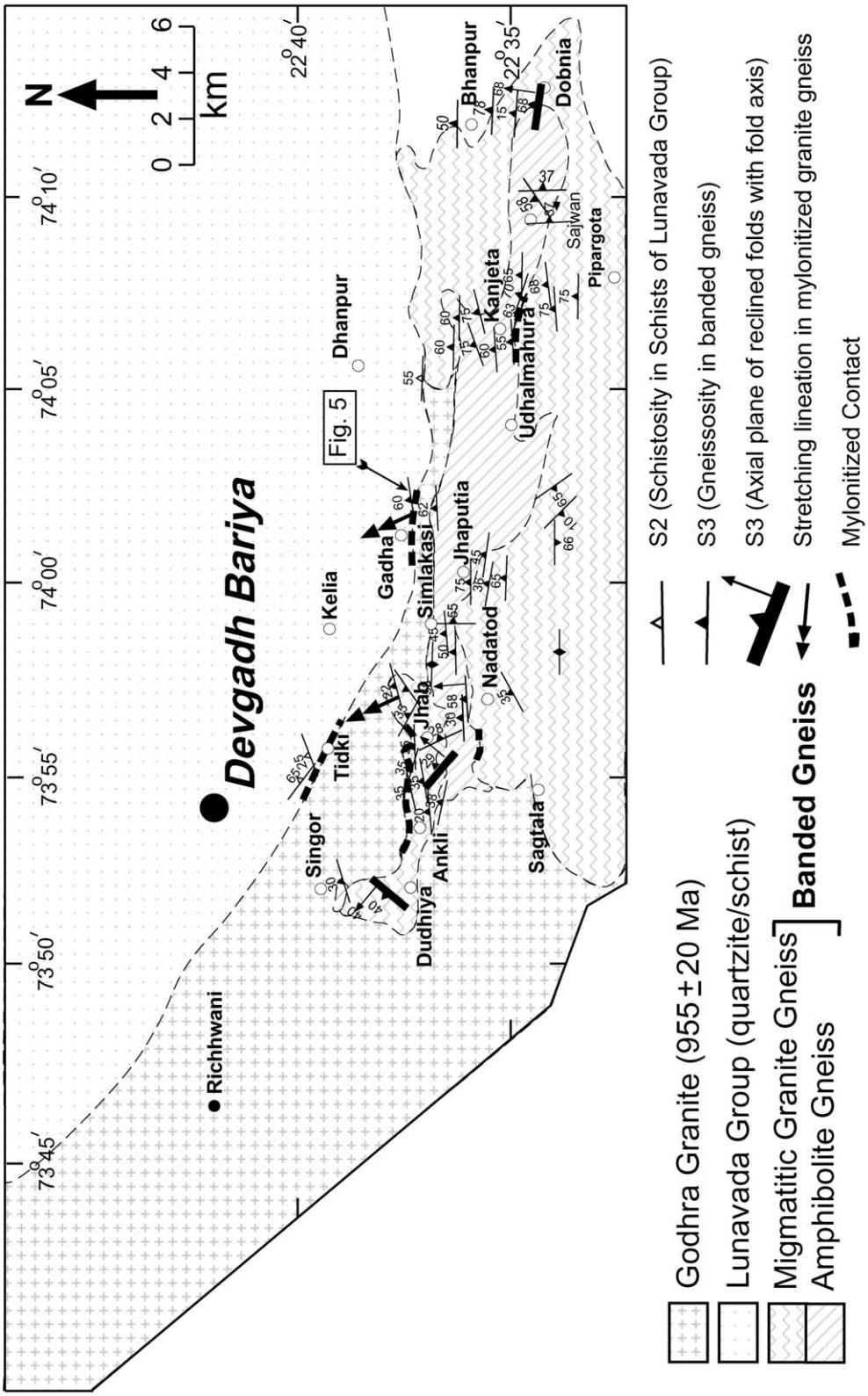

Fig. 4. Structural map of the study area. Location of Fig. 5 is shown.

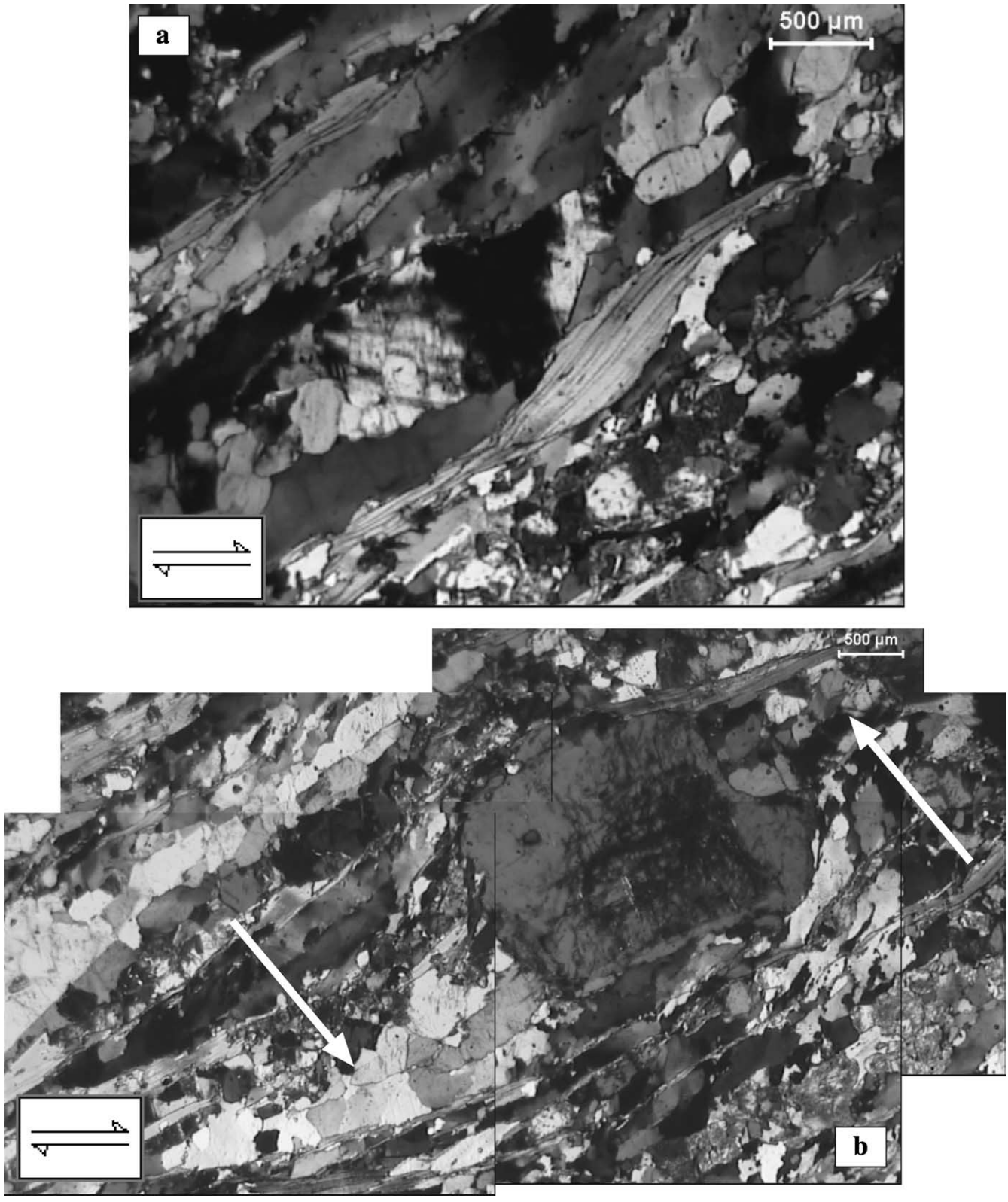

Fig. 5. Shear sense indicators in mylonitized granite gneiss occurring at contact with the metasedimentary rocks of the Lunavada Group (see Fig. 4 for location). Top of photomicrographs is toward the southeast. (a) Mica fish (muscovite); (b) asymmetric quartz pressure shadows around feldspar porphyroclast (white arrows point towards the pressure shadows).

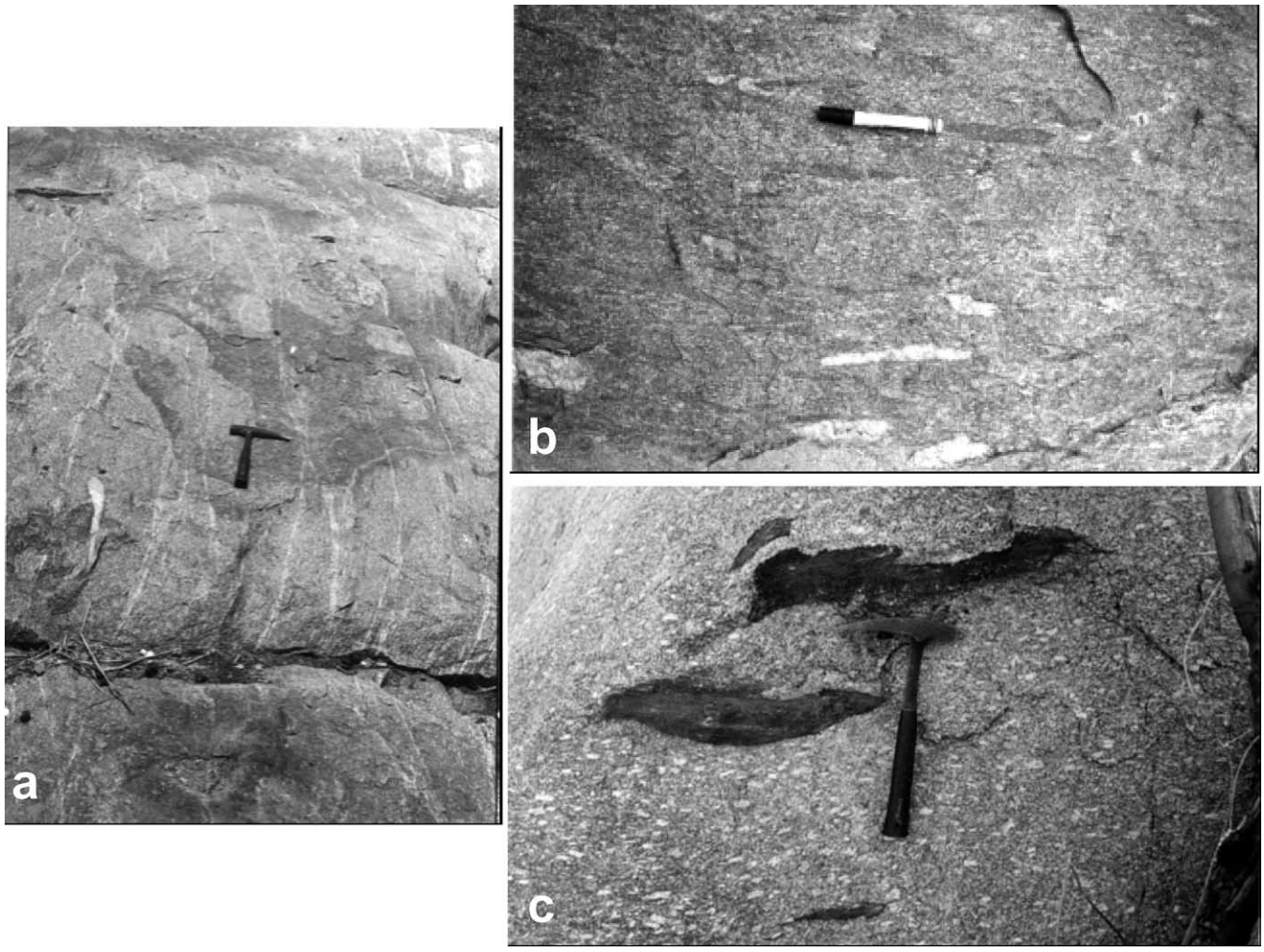

Fig. 6. Field fabrics in banded gneiss occurring at the southern margin of the granite. (a) and (b) are from near Ankli and (c) is 300 m south of Tidki (see Fig. 4). (a) Continuous bands of mica rich and quartz-feldspar rich layers at about 300 m from granite contact. Note the absence of mesoscopic folds. (b) Pinching out of feldspar-enriched bands in gneiss near the contact with the granite. (c) Mesoscopic foliation in the granite defined by parallel alignment of feldspar laths and mica and the presence of enclaves of banded gneiss.

fabric was gradually overprinted by a submagmatic stage high-T solid-state fabric.

5. Anisotropy of magnetic susceptibility

Having demonstrated that the Godhra Granite preserves deformational fabrics, it is now important to determine whether and how this fabric is related to the regional deformation recorded in the gneiss. Since the granite did not develop a well-mappable mesoscopic foliation, except in areas close to the margin, anisotropy of magnetic susceptibility (AMS) studies were carried out to determine the internal fabric. AMS is a widely accepted technique and a number of studies have investigated the relationship between AMS fabric and strain (e.g. Hrouda and Janak, 1976; Borradaile and Alford, 1987; Borradaile, 1988; Rochette et al., 1992; Hrouda, 1993; Tarling and Hrouda, 1993; Borradaile and Henry, 1997; Mamtani et al., 1999a; Mukherji et al., 2004). Particularly useful in structural geological work is the observation that the AMS ellipsoid is mostly correlatable with the strain ellipsoid. The three principal axes of the AMS ellipsoid ($K_1 \geq K_2 \geq K_3$) also define a magnetic lineation (K_1) and a magnetic foliation (plane containing K_1 and K_2; K_3 is the pole to foliation). AMS has also been used to constrain the kinematics of magma emplacement (Bouchez et al., 1990; Bouchez, 1997; Hrouda et al., 1999; McNulty et al., 2000). In the present study, the main objective was to establish a database of the magnetic foliation and lineation preserved in the granites and compare this with the magnetic and field fabrics in the gneiss. This database is then used to decipher the timing of granite emplacement and its deformation with reference to the deformation recorded in the gneiss.

5.1. Sampling and measurement

Oriented samples from 45 sites, 32 from the granites and

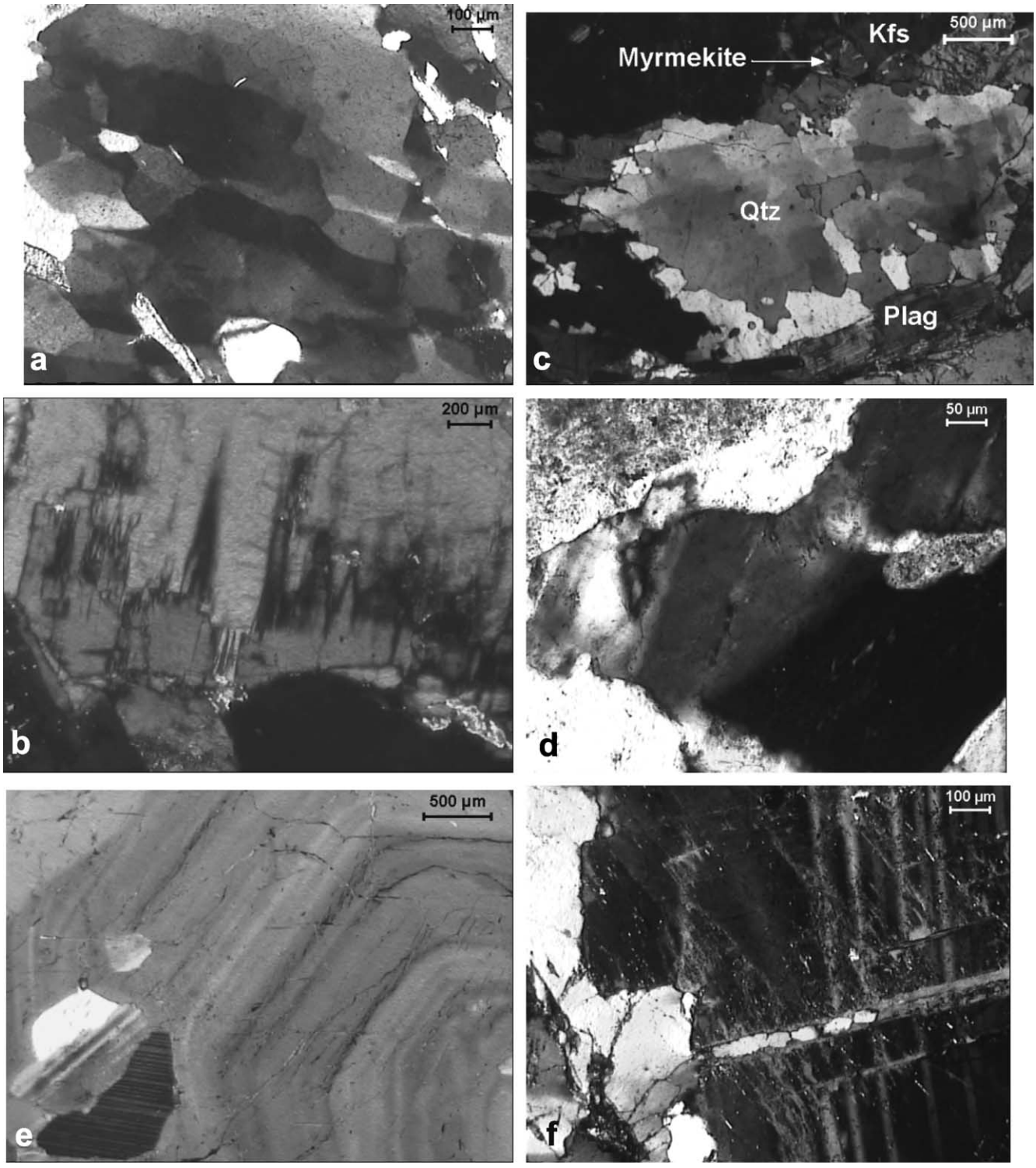

Fig. 7. (a)–(d) Solid-state deformation microstructures in Godhra granite. (a) Chess-board microstructure in quartz. (b) Deformation twins in feldspar. (c) Myrmekite lenses adjacent to K-feldspar (Kfs) and presence of subgrains in quartz; Plag is plagioclase. (d) Deformed and recrystallized feldspar. (e) Zoning in feldspar phenocryst. (f) Fractured feldspar filled with quartz.

13 from the gneiss, were collected from the area (Fig. 8). Each sample was at least 15 cm × 10 cm × 5 cm in size (Tarling and Hrouda, 1993). This size enabled drilling of an average of three cylindrical specimens per sample, each having 25.4 mm diameter and 22 mm height. A total of 139 cylindrical specimens were analyzed using the susceptibility meter (KLY-2 Kappabridge, AGICO, Czech Republic) of the Magnetic Laboratory of the University of Heidelberg (Germany). Measurements were made in the low magnetic field ($\pm 4 \times 10^{-4}$ T and 920 Hz). The susceptibility is

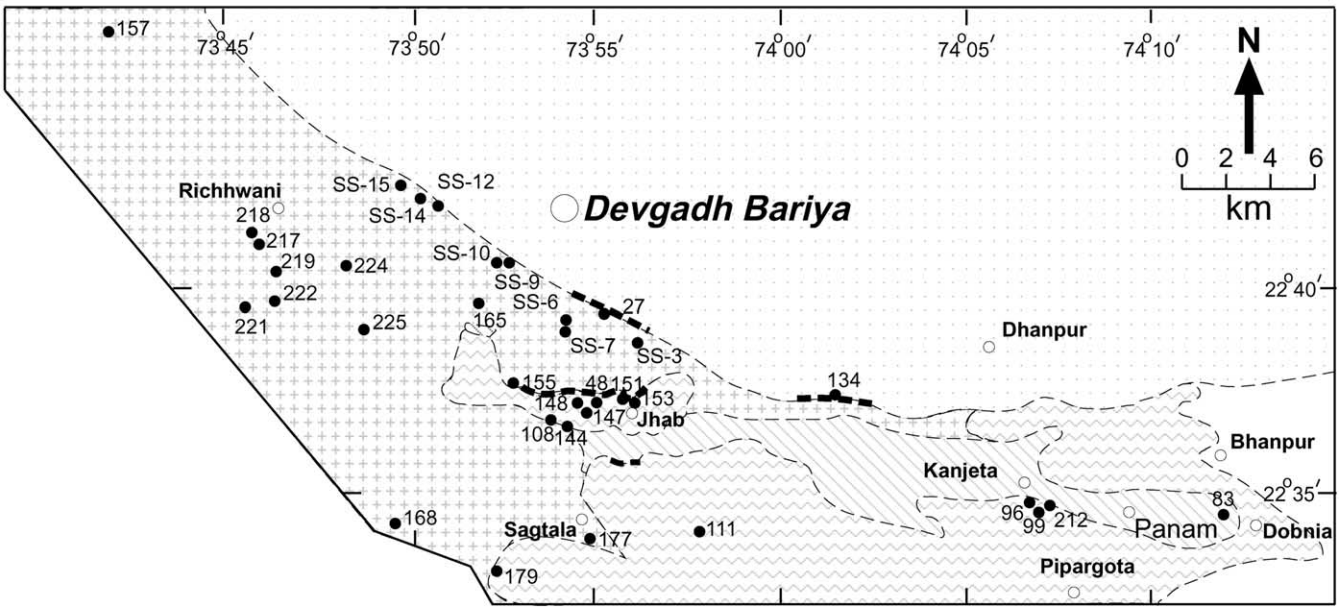

Fig. 8. Location map of samples taken for AMS study. Note: all the sample numbers without the prefix SS have a prefix MAM as listed in Table 1.

measured in 15 different directions of the sample to calculate the orientation and magnitude of the three principal axes of the magnetic susceptibility ellipsoid from which the mean susceptibility ($K_m = 1/3\ (K_1 + K_2 + K_3)$) is derived. The shape parameter T and the degree of magnetic anisotropy P' are both calculated after Jelinek (1981) and the formulae are given below:

$$T = (2\eta_2 - \eta_1 - \eta_3)/(\eta_1 - \eta_3)$$

$$P' = \exp\sqrt{\{2[(\eta_1 - \eta_m)^2 + (\eta_2 - \eta_m)^2 + (\eta_3 - \eta_m)^2]\}}$$

where $\eta_1 = \ln K_1$, $\eta_2 = \ln K_2$, $\eta_3 = \ln K_3$ and $\eta_m = (\eta_1 \cdot \eta_2 \cdot \eta_3)^{1/3}$.

Whilst T determines the shape of the susceptibility ellipsoid (prolate/oblate), P' is a measure of the eccentricity of the ellipsoid and is commonly used to gauge strain (Tarling and Hrouda, 1993).

5.2. AMS data

The data obtained by analysis of 139 cylindrical cores are listed in Table 1. The mean susceptibility values (K_m) of the porphyritic granite vary between 70 and $24{,}000 \times 10^{-6}$ SI but mostly range from 70 to 300×10^{-6} SI. Some porphyritic samples have K_m higher than 4000×10^{-6} SI and one sample (MAM-224) has a very high value around $24{,}000 \times 10^{-6}$ SI. The fine-grained granites generally have higher mean susceptibilities, mostly higher than 1000×10^{-6} SI and as high as $18{,}000 \times 10^{-6}$ SI; however, a couple of fine-grained granite samples have K_m lower than 100×10^{-6} SI. The mylonitized granite at the northern margin of the Godhra Granite has a lower susceptibility, 62×10^{-6} SI at a maximum. In comparison with this, the mylonitized banded gneiss occurring at the southern margin of the granite has a relatively high susceptibility of the order of $1000–2000 \times 10^{-6}$ SI or more. The migmatitic layers of the banded gneiss have K_m values around 4000×10^{-6} SI, the amphibolite parts have lower susceptibilities, ranging between 161 and 207×10^{-6} SI, but for one sample for which $K_m > 500 \times 10^{-6}$ SI. Fig. 9 shows histograms of K_m values for the different lithologies of the study area.

It is known that paramagnetic, diamagnetic and ferromagnetic minerals contribute to the rock susceptibility and to its anisotropy (Rochette, 1987). It is clear that in the low susceptibility samples, a paramagnetic mineral like biotite is the important contributor. However, the high susceptibility of some samples ($K_m > 500 \times 10^{-6}$ SI) must be on account of ferromagnetic minerals such as magnetite (Bouchez, 1997). The latter was determined by analyzing the temperature variation of magnetic susceptibility of powders from high susceptibility samples, using the CS-2 furnace (from room temperature to 700 °C) and the CS-L cryostat (from −196 to 0 °C temperature) attached to the KLY-2 Kappabridge. In high susceptibility samples, a sharp drop takes place at around 580 °C. This is the Curie temperature of magnetite and therefore it is confirmed that magnetite is an important carrier in our high susceptibility samples. However, magnetite can be single domain (SD) or multidomain (MD), and deciphering this is essential because SD magnetite can result in an inverse fabric wherein the orientation of K_1 and K_2 axes are interchanged (Rochette et al., 1992). In our high-susceptibility samples, the cooling experiments reveal a sharp drop in susceptibility at ∼−155 °C (Fig. 10a). This is referred to as the Verwey transition. Since from the heating experiments it was established that magnetite is an important phase of the samples, the Verwey transition in the cooling experiments is

Table 1
AMS data from Godhra Granite and associated gneiss, southern parts of Aravalli Mountain Belt (India)

Sample no.	K_m (10^{-6} SI)	P'	T	K_1	K_3
Porphyritic granite					
MAM-27.1	166.36	1.077	−0.018	314/18	213/29
MAM-27.2	158.04	1.075	0.068	315/21	211/31
MAM-108.1	7909.08	1.221	0.677	94/16	185/2
MAM-108.2	5463.08	1.159	0.565	278/3	188/5
MAM-157.1	296.68	1.122	0.079	320/43	158/46
MAM-157.2	312.54	1.132	0.168	323/43	163/45
MAM-157.3	307.68	1.129	0.139	327/39	164/50
MAM-164.1	2375.88	1.054	0.439	69/0	159/29
MAM-164.2	2527.88	1.054	0.367	270/11	171/38
MAM-165A.1	259.82	1.049	0.391	267/40	160/18
MAM-165A.2	258.99	1.049	0.741	268/37	155/27
MAM-165A.3	293.26	1.046	0.088	269/27	165/25
MAM-165B.1	254.08	1.052	0.446	69/16	170/33
MAM-165B.2	254.96	1.058	0.370	266/16	168/24
MAM-165B.3	292.39	1.041	0.489	77/22	173/15
MAM-177.1	4182.80	1.150	−0.408	337/75	185/13
MAM-177.2	3833.80	1.171	−0.370	285/72	188/2
MAM-177.3	4090.13	1.192	−0.228	275/69	182/1
MAM-218.1	3119.80	1.191	0.208	268/20	134/62
MAM-218.2	3061.93	1.266	0.600	277/37	160/31
MAM-219.1	12666.47	1.148	−0.009	111/2	15/68
MAM-219.2	5093.80	1.084	−0.490	278/7	8/2
MAM-222A.1	210.17	1.053	0.537	320/13	65/49
MAM-222A.2	166.68	1.061	0.374	324/8	60/32
MAM-224.1	6959.13	1.095	0.118	286/16	160/64
MAM-224.2	20218.47	1.247	0.667	300/19	161/66
MAM-224.3	23982.46	1.268	−0.038	287/27	172/40
MAM-225.1	197.62	1.051	0.077	334/54	153/36
MAM-225.2	166.25	1.071	0.392	8/44	154/41
MAM-225.3	168.18	1.045	0.133	351/49	163/40
SS-2.1	195.63	1.080	0.009	29/50	212/40
SS-2.2	179.17	1.078	−0.014	22/51	211/39
SS-3.1	174.20	1.062	−0.254	281/10	98/80
SS-3.2	188.70	1.068	−0.286	279/9	152/75
SS-3.3	191.12	1.068	−0.269	289/14	144/73
SS-3.4	181.56	1.063	−0.383	275/2	171/84
SS-5.1	181.22	1.091	−0.316	312/11	210/45
SS-5.2	193.71	1.079	−0.628	132/0	222/32
SS-5.3	179.66	1.086	−0.285	311/9	210/51
SS-5.4	179.34	1.079	−0.567	310/1	219/52
SS-6.1	74.12	1.077	−0.458	322/18	54/5
SS-6.2	73.16	1.083	−0.343	322/17	230/5
SS-6.3	76.96	1.091	−0.079	134/5	227/28
SS-6.4	70.46	1.077	−0.467	309/1	218/25
SS-6.5	76.11	1.079	−0.416	323/14	233/1
SS-6.6	74.84	1.082	−0.319	132/2	222/13
SS-7.1	94.25	1.105	0.303	18/13	111/12
SS-7.2	91.87	1.107	0.430	18/16	112/15
SS-7.3	89.57	1.107	0.637	11/24	107/12
SS-9.1	83.04	1.075	0.296	95/5	193/56
SS-9.2	101.55	1.092	0.301	94/16	348/43
SS-9.3	101.83	1.094	0.262	79/11	339/40
SS-10.1	111.24	1.043	0.241	266/24	67/64
SS-10.2	88.25	1.087	0.319	77/35	308/42
SS-10.3	113.88	1.046	0.303	269/21	53/65
SS-12.1	85.07	1.087	−0.352	141/9	240/47
SS-12.2	94.99	1.093	−0.385	314/4	219/48
SS-12.3	102.51	1.093	−0.409	316/0	226/31
SS-14.1	83.00	1.077	−0.377	178/11	269/7
SS-14.2	92.27	1.077	−0.412	181/19	89/4
SS-14.3	91.86	1.066	−0.441	177/6	268/13
SS-14.4	86.38	1.075	−0.419	180/23	270/1

Table 1 (*continued*)

Sample no.	K_m (10^{-6} SI)	P'	T	K_1	K_3
SS-15.1ag	86.00	1.130	0.396	308/17	191/56
SS-15.2	83.16	1.132	0.396	308/16	190/58
Fine-grained granite					
MAM-99.1	14413.09	1.415	−0.113	307/61	198/11
MAM-99.2	18021.08	1.407	−0.113	301/70	190/7
MAM-99.3	16027.75	1.405	−0.085	289/64	189/5
MAM-99b.1	13973.65	1.394	0.031	283/60	181/7
MAM-99b.2	15184.32	1.388	−0.191	315/62	202/12
MAM-99b.3	13439.65	1.419	−0.166	293/52	183/15
MAM-111.1	97.42	1.071	0.362	241/33	2/39
MAM-111.2	99.10	1.074	0.388	236/34	354/34
MAM-111.3	98.58	1.070	0.243	241/37	3/36
MAM-111.4	98.24	1.067	0.258	244/38	12/39
MAM-144.1	4055.42	1.200	0.160	286/40	164/32
MAM-144.2	4825.75	1.291	0.465	290/43	163/33
MAM-144.3	5474.75	1.263	0.350	298/51	159/31
MAM-144.4	4256.42	1.239	0.273	299/51	163/30
MAM-144b.1	5149.08	1.218	0.346	289/35	147/48
MAM-144b.2	2483.08	1.128	0.080	301/56	154/29
MAM-144b.3	3685.75	1.190	0.126	291/57	142/29
MAM-155.1	4597.75	1.578	0.510	110/40	350/30
MAM-158.1	1460.17	1.065	0.394	86/13	176/1
MAM-158.2	1365.63	1.073	0.376	93/25	186/6
MAM-158.3	1699.30	1.084	−0.073	89/6	181/15
MAM-168.1	92.15	1.122	0.695	43/26	169/50
MAM-168.2	88.64	1.122	0.774	35/38	168/41
MAM-168.3	87.62	1.104	0.633	45/22	164/50
MAM-179.1	2534.98	1.106	0.453	279/33	177/18
MAM-179.2	2751.92	1.109	0.277	276/27	181/10
MAM-179.3	2163.92	1.108	0.365	277/30	173/24
MAM-217.1	10432.47	1.264	0.324	349/63	155/26
MAM-217.2	9699.13	1.248	0.477	310/62	147/27
MAM-217.3	10332.47	1.305	0.353	344/62	141/27
MAM-217.4	9930.47	1.253	0.393	339/62	158/28
MAM-221.1	54.90	1.041	−0.196	119/9	209/1
MAM-221.2	57.07	1.034	0.025	118/5	28/0
MAM-221.3	55.86	1.043	−0.063	113/20	203/1
SS-17.1	12885.75	1.176	0.642	21/55	177/33
SS-17.2	12707.75	1.175	0.587	17/57	184/32
SS-17.3	11759.75	1.145	0.280	8/62	197/28
SS-17.4	12938.42	1.202	0.398	229/55	185/32
Mylonitic rocks at granite contact					
MAM-48.1	2227.48	1.300	0.627	279/20	173/37
MAM-48.2	1030.55	1.176	0.416	281/10	181/44
MAM-48.3	968.55	1.177	0.607	278/2	186/47
MAM-48.4	1070.55	1.182	0.449	282/5	186/47
MAM-134.1	43.75	1.047	0.196	269/55	174/4
MAM-134.2	36.36	1.042	0.302	293/56	164/23
MAM-134.3	53.12	1.043	0.237	277/73	162/7
MAM-134.4	60.24	1.061	0.261	93/79	337/5
MAM-134.5	42.04	1.040	0.343	281/49	161/23
MAM-134.6	62.38	1.047	0.505	252/73	158/1
MAM-147.1	9584.42	1.227	0.552	89/0	179/25
MAM-147.2	4705.08	1.210	0.829	79/38	188/22
MAM-148.1	1339.82	1.101	0.569	243/25	150/6
MAM-148.2	1294.55	1.102	0.419	240/12	148/10
MAM-148.3	1554.75	1.093	0.493	238/15	146/6
MAM-151L.1	1018.95	1.333	0.572	329/26	204/50
MAM-151L.2	918.55	1.292	0.575	326/29	175/58
MAM-151L.3	806.88	1.291	0.510	325/29	195/49
MAM-151.1	1870.85	1.349	0.544	320/26	159/63

(*continued on next page*)

Table 1 (*continued*)

Sample no.	K_m (10^{-6} SI)	P'	T	K_1	K_3
MAM-151.2	2842.85	1.449	0.358	329/25	168/64
MAM-151.3	1422.85	1.354	0.582	322/27	164/62
MAM-151.4	1366.18	1.361	0.478	328/23	164/66
MAM-153.1	351.08	1.233	0.845	98/12	211/62
MAM-153.2	379.18	1.227	0.851	121/0	212/66
MAM-153b.1	1457.22	1.287	0.701	326/31	177/54
MAM-153b.2	1609.62	1.271	0.867	326/26	184/58
Migmatitic granite gneiss (part of banded gneiss)					
MAM-123.1	132.14	1.182	0.771	274/53	170/10
MAM-123.2	137.55	1.156	0.692	280/51	170/16
MAM-212.1	4041.65	1.565	0.154	298/71	180/9
MAM-212.2	4546.32	1.723	0.131	303/75	178/9
MAM-212.3	3928.98	1.591	0.055	298/69	179/11
MAM-212.4	4891.32	1.536	0.087	302/69	177/12
Amphibolite gneiss (part of banded gneiss)					
MAM-83.1	576.05	1.148	0.961	276/9	183/19
MAM-83.2	2023.22	1.211	0.644	263/56	356/2
MAM-90.1	175.79	1.017	0.507	71/35	178/22
MAM-90.2	161.52	1.025	0.176	65/48	256/42
MAM-96.1	174.32	1.033	0.470	305/32	187/37
MAM-96.2	149.53	1.038	0.227	308/47	190/24
MAM-96.4	207.57	1.049	0.442	301/37	185/30

K_m, mean susceptibility; P', corrected degree of anisotropy; T, shape parameter; K_1 and K_3, respectively, are the azimuth/inclination of maximum and minimum axis of the magnetic susceptibility ellipsoid. Note: In the sample numbers, the figure after the point indicates the core number.

concluded to be due to a change of lattice symmetry in magnetite (Tarling and Hrouda, 1993). This is characteristic of MD-magnetite. Thus, it is established that the high susceptibility of our samples is due to MD-magnetite. Petrographic analysis of high-susceptibility samples also confirmed the presence of magnetite grains as big as 0.3 mm. The large size proves that MD-magnetite is an important contributor to the high susceptibility values of such granites (Fig. 10b). Temperature variation of magnetic susceptibility experiments were also carried out on samples that have low magnetic susceptibility (paramagnetic granites) and it was found that these samples do not contain magnetite (Fig. 10c); a petrographic study of such samples also did not reveal any presence of magnetite (Fig. 10d).

The shape of the susceptibility ellipsoid is studied by plotting the anisotropy degree (P') against the shape parameter (T). Separate plots were prepared for the different rock types, viz. porphyritic granite (Fig. 11a), fine-grained granite (Fig. 11b), mylonitic granite margin rocks (Fig. 11c), migmatitic granite gneiss (Fig. 11d) and amphibolite gneiss (Fig. 11e). It is found that most of the samples have an oblate susceptibility ellipsoid (Fig. 11). The anisotropy degree of the migmatitic granite gneiss (Fig. 11d) is higher than that of the granite. Similarly, the mylonites that outcrop at the margin of the granite (Fig. 11c) also tend to have higher anisotropy degrees. Interestingly, prolate ellipsoids occur in a few porphyritic granites (Fig. 11a), mostly from the northern margin of the granite, where it is in contact with the Lunavada metasedimentary rocks. The shape of the susceptibility ellipsoid has in some earlier studies been correlated with the shape of the strain ellipsoid (e.g. Borradaile and Alford, 1987; Tarling and Hrouda, 1993). Although this is a complex relationship, the presence of prolate susceptibility ellipsoids in some of the granite margin rocks could imply that locally, the granite underwent a more linear strain.

Fig. 12a is the magnetic foliation map for the area and Fig. 12b is the pole-diagram (K_3) for the magnetic foliations. Fig. 13a is the magnetic lineation map (K_1) and Fig. 13b is the orientation diagram of the magnetic lineation in the granite.

6. Discussion

6.1. Syntectonic emplacement of the Godhra Granite

Microstructures in the granites close to the margin, as well as away from it, reveal high temperature solid-state deformation features. It is therefore inferred that the Godhra Granite is deformed in the solid state. With this background it is now possible to correlate the magnetic and the field fabrics in order to understand whether there is any relation between the regional strain/kinematics and fabric development in the granites. The magnetic foliations in the granite are parallel to both the magnetic foliations (Fig. 12b) and to field foliations of the gneiss (compare Figs. 12b and 3b). Moreover, the magnetic lineation dominantly plunges in the NW direction (Fig. 13b) as does the stretching lineation in the mylonites and the D_3 fold axes in the gneiss (Fig. 4).

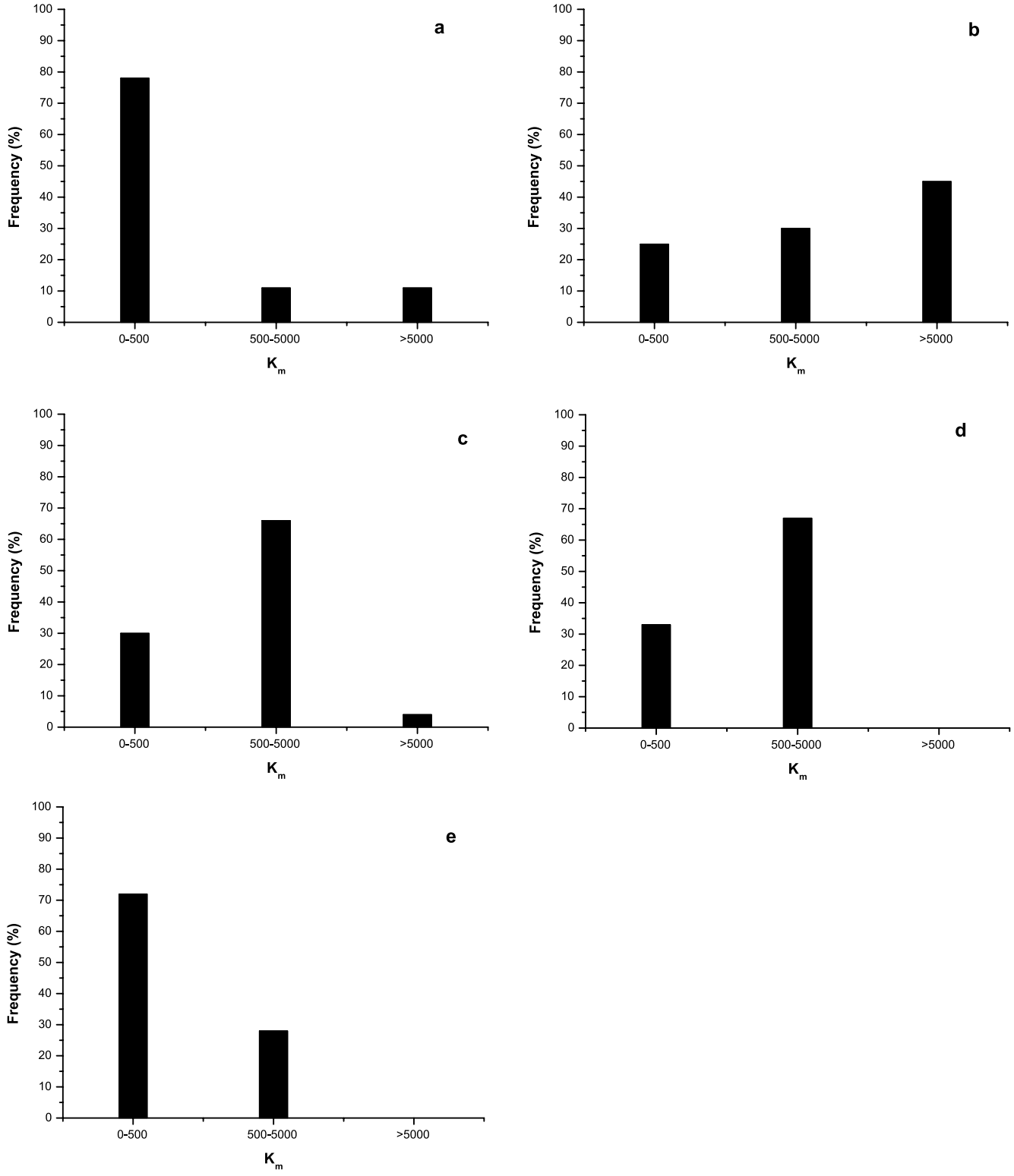

Fig. 9. Histograms showing frequency distribution of mean susceptibility (K_m) in (a) porphyritic granite, (b) fine-grained granite, (c) mylonitic rocks at margin of granite, (d) migmatitic granite gneiss, and (e) amphibolite gneiss.

Therefore, it is inferred that the granite accommodated strain related to D_3 deformation in the gneiss.

Paterson et al. (1989) have argued that such plutons usually contain parallel or sub-parallel magmatic and high temperature solid-state fabrics. It is therefore important to show that the solid-state foliation in the pluton developed during and not after emplacement, by obtaining evidence of high-T solid-state deformation and/or synmagmatic flow

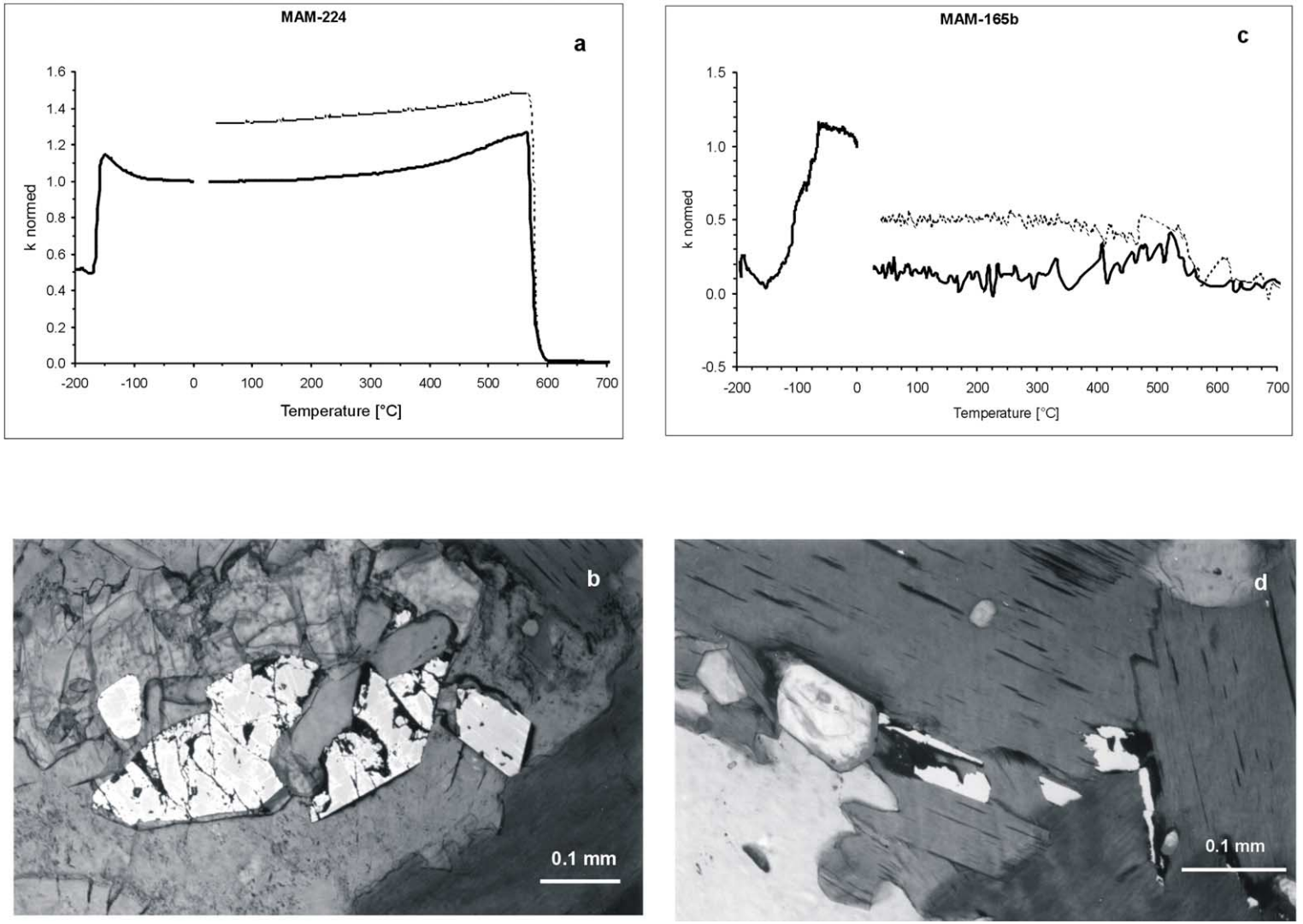

Fig. 10. (a) *K–T* curve obtained for a ferromagnetic granite (Sample MAM-224) documenting the presence of multidomain (MD) magnetite as an important mineral phase. (b) Photomicrograph of the above ferromagnetic granite sample (MAM-224) taken under reflected light showing the presence of a large magnetite grain, thus confirming the presence of MD magnetite. (c) *K–T* curve obtained for a paramagnetic granite (Sample MAM-165b) documenting the absence of magnetite in this low susceptibility sample. (d) Photomicrograph of the paramagnetic granite (MAM-165b) taken under reflected light; magnetite is clearly absent here.

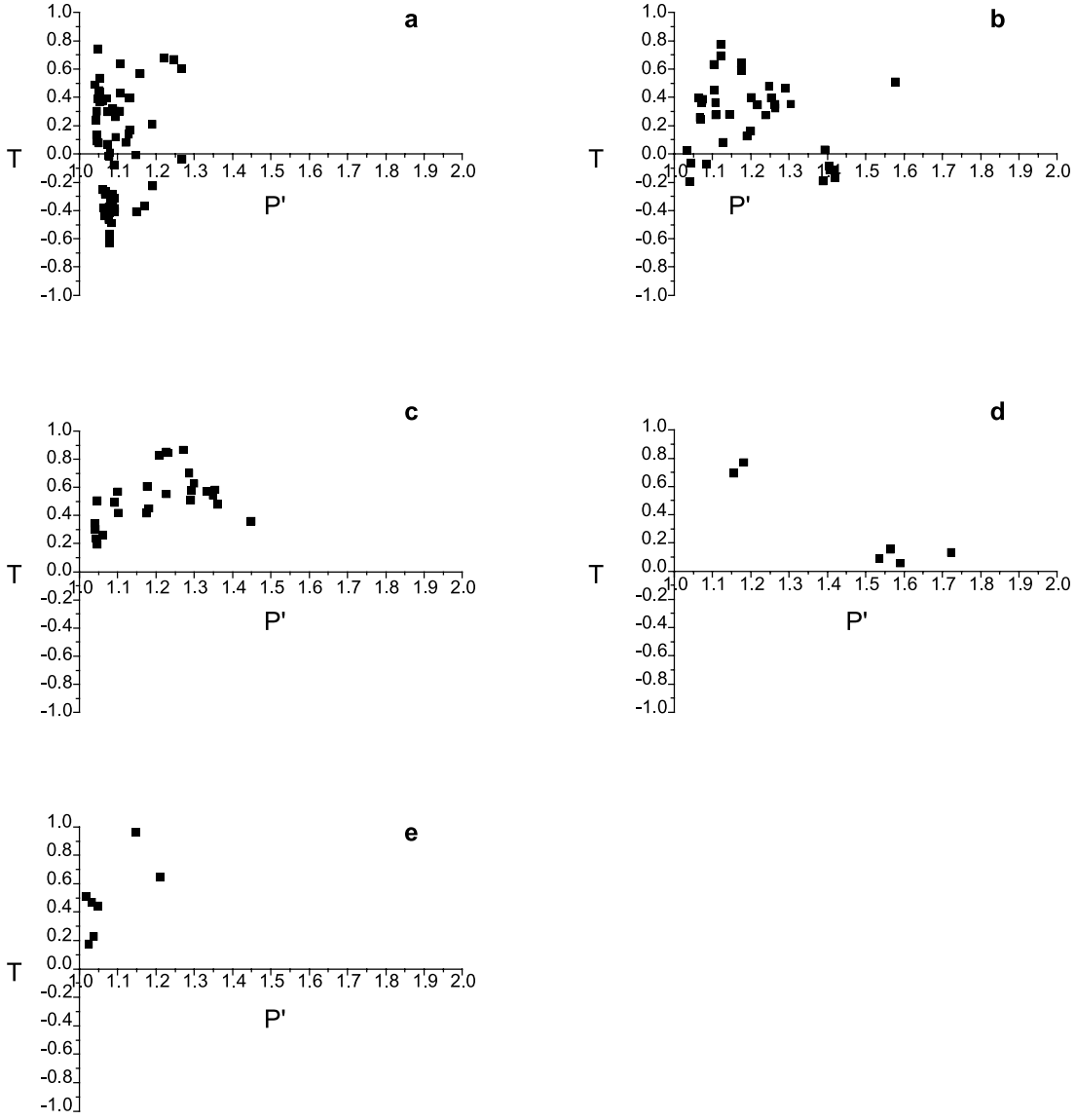

Fig. 11. T, P' plots (Jelinek plots) for porphyritic granite (a), fine-grained granite (b), mylonitic rocks at margin of granite (c), migmatitic granite gneiss (d) and amphibolite gneiss (e). Most of the samples except for a few porphyritic granites fall in the oblate field.

fabrics (McCaffrey et al., 1999). In our granite, evidence of synmagmatic deformation during emplacement is inferred from the gradual decrease in the intensity of field foliation in the granite from the margin to the interior. In some parts that are remote from the margin, the euhedral laths of feldspar define a field fabric, which indicates fabric formation during deformation of crystallizing magma (Paterson et al., 1989; Bouchez et al., 1990; Benn et al., 1998). Moreover, the presence of high-T solid-state deformation microstructures such as chessboard texture in quartz indicates that crystal plasticity began at temperatures close to the solidus (Mainprice et al., 1986; Paterson et al., 1989; Kruhl, 1996; Blenkinsop, 2000; Neves et al., 2003). Myrmekites bordering ductilely deformed feldspar and feldspars with quartz-filled fractures all indicate that strain developed under near-solidus conditions and that submagmatic deformation took place (Bouchez et al., 1990; McCaffrey et al., 1999). Therefore, based on the field and microstructural evidences mentioned above, it is inferred that the Godhra Granite is a syntectonic body that underwent synmagmatic deformation during its emplacement. It is concluded that there was a continuity from magmatic to solid-state deformation as the magma was emplaced and cooled. Such a synchronism between magma emplacement and tectonics has also been documented for other granite plutons (e.g. Saint-Blanquat and Tikoff, 1997; Alonso Olazabal et al., 1999; Greiling and Verma, 2001).

6.2. Emplacement during late stage deformation (D_3 in gneiss)

The evidence of solid-state deformation fabric in the

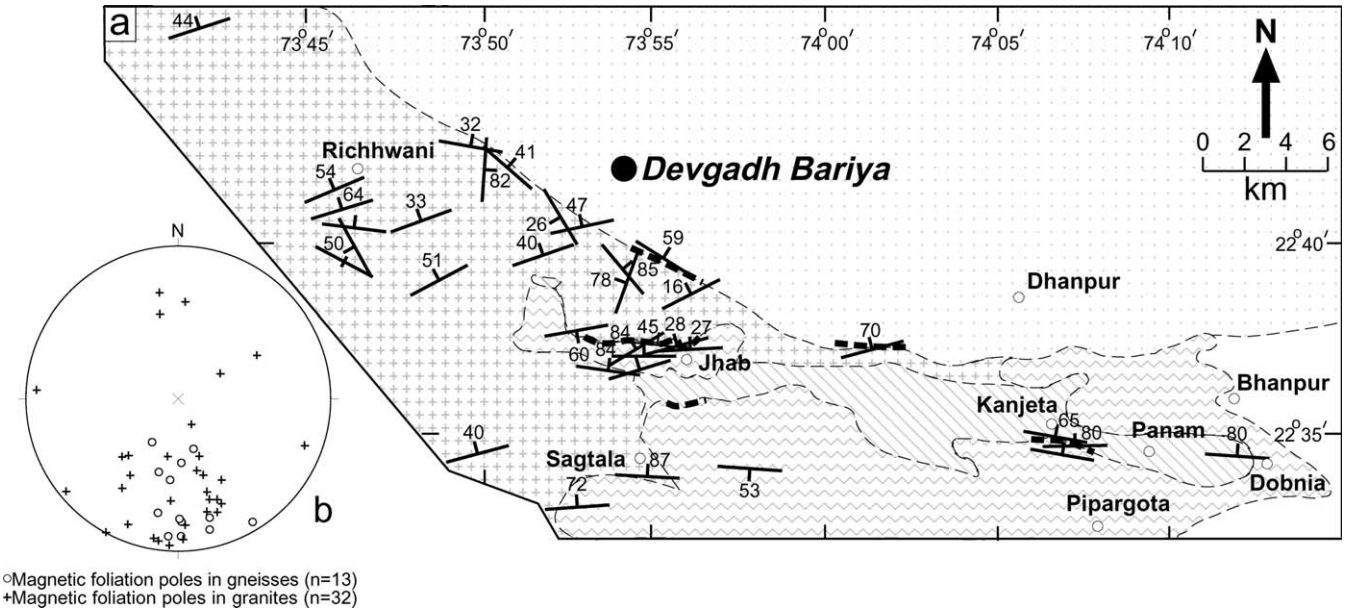

Fig. 12. (a) Magnetic foliation map of the study area. (b) Magnetic foliation poles (K_3) for granites and gneisses investigated in this study. Note the parallelism between magnetic foliation of granite and gneiss (compare with Fig. 3b).

granite implies that the magma must have had a high crystal percentage during its emplacement. There is a parallelism between the S_3 foliation in the gneiss and the magnetic foliation in the granite. Moreover, most of the magnetic lineations (Fig. 13b) plunge towards the NW, which is also the direction of plunge of the stretching lineations and D_3 fold axis lineations recorded in the gneiss. Therefore it is inferred that the magnetic fabric preserved in the granite is dominantly related to the D_3 deformation recorded in the gneiss. Moreover, the orientation of feldspar laths in the granite, wherever recorded, is noted to lie between W and WNW. This is sub-parallel to the D_3 field fabric in the gneiss and also to the magnetic fabric recorded in the granite as well as gneiss. As discussed earlier, the presence of preferentially aligned feldspar laths is taken as evidence of synmagmatic deformation. Therefore, it is inferred that the Godhra Granite underwent synmagmatic deformation during D_3. It is envisaged that the emplacement may have

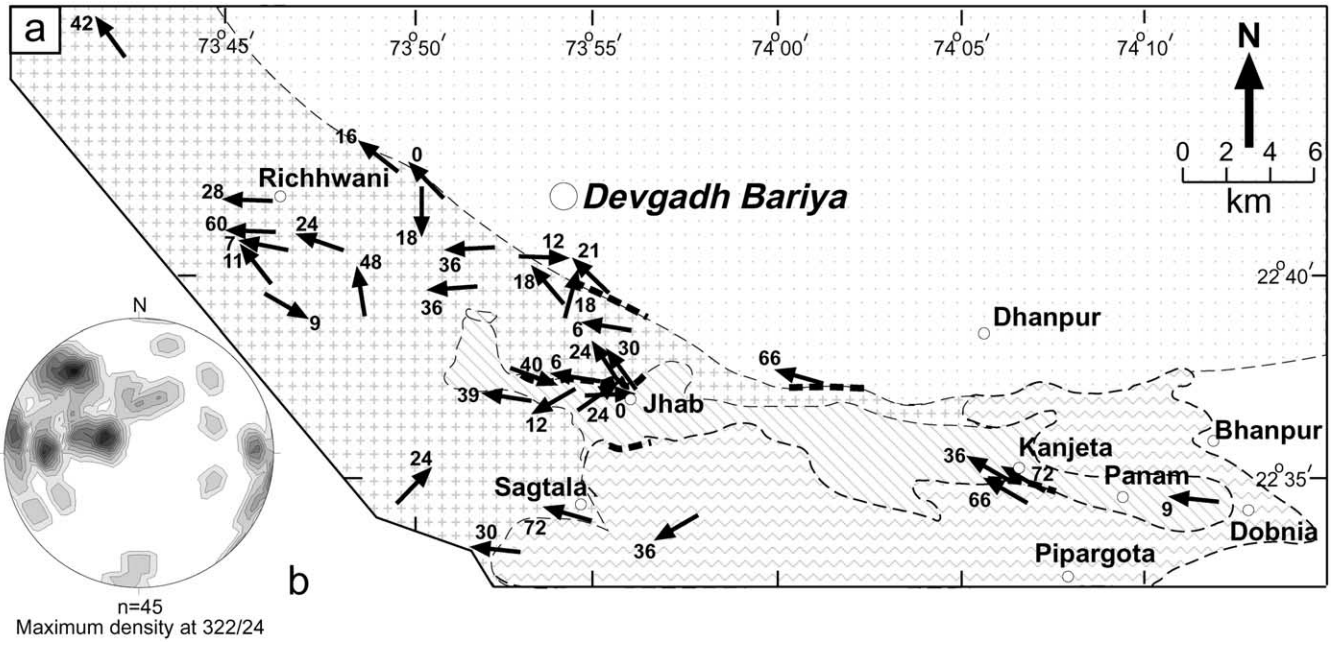

Fig. 13. (a) Magnetic lineation map of the study area. (b) Contoured lower hemisphere equal area projection of magnetic lineation (K_1) data from granite and gneiss with a maxima at 322/24 (NW direction). This NW plunge of K_1 is also the plunge of the stretching lineation of the mylonites (Fig. 4) and the orientation of D_3 fold axes lineation in the gneiss (Fig. 3a).

Table 2
Comparison of field structural data in the Banded Gneiss (present study) and the southern Aravalli metasedimentary rocks (Lunavada and Champaner Group) with data (field and magnetic) of the Godhra Granite

Banded gneiss	Southern Aravalli metasedimentary rocks		Godhra Granite
	Lunavada Group	Champaner Group	
D_1/D_2 (coaxial): rarely preserved	D_1/D_2 (coaxial)	Deformation equivalent to D_1/D_2 of gneiss or Lunavada Group is absent	No deformation equivalent to D_1/D_2 of gneiss or Lunavada Group
AP_2 = SW to WSW	AP_2 = SW		
FA_2 = NE	FA_2 = NE to SW		
D_3	D_3	D_1	Preferred orientation of feldspar laths: WNW to W
AP_3 = WNW to WSW	AP_3 = NW to W	AP_1 = WNW to W	MF strike = WNW to WSW
FA_3 = NW	FA_3 = NW	FA_1 = W	ML plunge = NW to W (maxima towards NW)

Data from Lunavada Group are after Mamtani et al. (1999a,b, 2000) and Champaner Group are after Merh (1995). AP, axial plane; FA, fold axis; MF, magnetic foliation; ML, magnetic lineation.

initiated during early D_3 and that most of the synmagmatic fabric developed during the main phase of D_3 deformation recorded in the gneiss.

6.3. Regional tectonics in the Southern Aravalli region, Rodinia Supercontinent and Godhra Granite

It is known that the southern part of the AMB, which comprises the banded gneiss, Lunavada Group, Champaner Group and Godhra Granite, has been affected by at least three deformation events. However, all the three deformation phases are not recorded in each stratigraphic unit, which has been used as a criterion to consider the stratigraphic position of some units (Roy, 1988; Gupta et al., 1995). Table 2 shows the deformation events recorded in different stratigraphic units of the region. Accordingly, it is noted that D_3 structures in the gneiss, D_3 structures in the Lunavada Group rocks and the (single phase) structures in the Champaner Group rocks have similar trends. The axial surfaces strike between WNW and WSW and the fold axes plunge in a general NW direction. As seen in Table 2, the magnetic fabric in the Godhra Granite is also correlatable to D_3 structures in the gneiss, to the D_3 structures in the Lunavada Group, and the structures in the Champaner Group of rocks. Therefore, it is inferred that the emplacement of the Godhra Granite was synchronous with the D_3 of the gneiss, and the last phase of deformation of the southern Aravalli metasedimentary rocks.

Besides the above, there are also other important regional tectonic implications of the present study. The age of the Godhra Granite is ~1 Ga (955 ± 20 Ma), which is a Grenvillian age (1.1–0.9 Ga; Condie, 2001) and it is known that Rodinia Supercontinent assembly took place during this Meso-Neoproterozoic period (Condie, 2001). Recent U–Pb geochronological studies on the Chang Pluton of the Sendra Granitoid Suite lying in the northern parts of the AMB have yielded an age of 967 ± 1.2 Ma (Pandit et al., 2003). Since this age is ~1 Ga these authors have suggested that the Aravalli region played an important role during Rodinia assembly. Geochronological studies on other granites of the Aravalli region have also yielded similar ages, e.g. the Ambaji Granite (~1228 Ma Rb–Sr age; Crawford, 1975) and the Sendra Granite (966 ± 250 Ma Rb–Sr age; Tobisch et al., 1994). Also, U–Pb zircon ages of 987 ± 6.4 and 986.3 ± 2.4 Ma have been obtained from rhyolites in the Ambaji–Sendra terrain lying in the central and northern parts of the Aravalli Mountain Belt (Deb et al., 2001). Besides this, there are other igneous rocks (diorites) in the Aravalli region that have yielded an Sm–Nd whole rock age of ~1 Ga (Volpe and Macdougall, 1990). All of the above imply that there is evidence of igneous activity during Grenvillian times (~1 Ga) in the Aravalli region. As stated in Section 1, the Godhra Granite has proximity to the CITZ in which Grenvillian age tectonothermal events have been noted (Yoshida et al., 2001; Bhowmik and Dasgupta, 2004). Muscovite and biotite from the schists of the Lunavada Group yielded Ar–Ar cooling ages between 947.3 ± 6.6 and 923.7 ± 5.0 Ma (unpublished data; collaborative research with W. Frank, Vienna, Austria). These are similar to the age of the Godhra Granite, both being ~1 Ga (Grenvillian). Although the Godhra Granite was dated using the Rb–Sr technique, a similar Ar–Ar cooling age in mica from schists of the Lunavada Group implies that the southern Aravalli region was affected by a deformation and associated recrystallization (tectonothermal) event at ~1 Ga. This also implies that after the ~1 Ga event, there was no major tectonothermal event in the southern parts of the AMB; otherwise, the Ar–Ar system would have been reset to younger ages. In light of this, the ~1 Ga age of the Godhra Granite, though based on the Rb–Sr method, becomes reliable and also very important. It is inferred that the deformation event at ~1 Ga also controlled the fabric development in the Godhra Granite. As discussed above, since this is the age of Rodinia Supercontinent assembly, it is inferred that the emplacement of the Godhra Granite, tectonothermal evolution of the southern Aravalli region and Grenvillian age tectonothermal events along the CITZ are related to the build up of the Rodinia

Supercontinent. This calls for further geochronological studies on the rocks of the region, especially the banded gneiss, to supplement this inferred relationship.

6.4. Emplacement mechanism of the Godhra Granite

In the banded gneiss, the D_3 reclined folds have axes that plunge due NW and it has been shown that ductile shearing took place during this deformation event. The stretching lineations recorded in the gneiss are parallel to the fold axes of the D_3 folds. Thus, the stretching lineation is not parallel to the strike of the S_2/S_3 foliation recorded in the gneiss. As a result, it is inferred that oblique simple shear was important during D_3 deformation of the gneiss. As discussed in Section 6.3, the emplacement of the Godhra Granite is inferred to be synchronous to D_3 deformation of the gneiss and the last deformation event of the Aravalli Supergroup rocks. It is known from previous studies that these last generation folds in the Aravalli Supergroup rocks (D_3 folds in Lunavada Group and the folds in the Champaner Group) are symmetrical (Merh, 1995; Mamtani et al., 2000). This implies the presence of a horizontal shortening component during their development. Thus it is inferred that during the emplacement of the Godhra Granite, on a regional scale, there must have been a horizontal shortening component whilst locally the granitoids were subjected to ductile shearing by oblique simple shear.

Oblique simple shear can occur in zones of transpression (Jones and Holdsworth, 1998) and there are previous studies that provide evidence for a close relationship between granite plutons, shear zone systems and transpressive convergent zones (D'Lemos et al., 1992; Ingram and Hutton, 1994; Brown and Solar, 1998a,b; Pressley and Brown, 1999; Greiling and Verma, 2001). It is believed that crustal thickening during transpressive orogenesis can produce anatectic granites and can localize deformation thus leading to transcurrent movement (D'Lemos et al., 1992). It has also been argued that granites can migrate from their source to the mid-crust through relatively narrow shear zones. Vigneresse and Tikoff (1999) and Vigneresse and Clemens (2000) have argued that deformation is necessary for magma ascent. According to Vigneresse and Tikoff (1999), strain partitioning causes horizontal migration of melt into shear bands while the shear bands act as vertical conduits allowing melt migration to higher structural levels. Deformation-assisted pumping of melt is believed to be the mechanism by which this upward migration can take place. According to Dewey et al. (1998), transpression is defined as a strike-slip deformation that deviates from simple shear due to a component of shortening orthogonal to a steeply dipping or sub-vertical deformation zone. In the granitoids of the study area it is found that the D_3 folds plunge due NW and the stretching lineation that marks the extension directions also plunges in the NW direction. It is known that during transpression, fold-axis parallel extension is a common feature (Jamison, 1991; Benn et al., 1998). However, the basic definition of transpression requires that the foliations should be vertical or steeply dipping (also see Fossen and Tikoff, 1998; Saint-Blanquat et al. 1998). In the granitoids of the study area, although vertical foliations are noted at a few places, the majority of them are moderate to gently plunging (Fig. 3). Therefore, the authors have refrained from using the term 'transpression' in the present study and oblique simple shear in the gneiss is inferred to have been the dominant mechanism. It is envisaged that the foliations and shear zones in the gneiss acted as pathways for the granitic melt migration in an oblique simple shear setting, thus allowing the melt to rise upwards towards higher crustal levels during D_3 deformation.

Emplacement of granitic plutons can also take place as expanding or ballooning diapirs (Paterson et al., 1989). During final emplacement, such diapirs balloon and develop a solid-state foliation in their solidified outer portion. Such a solid-state foliation at near emplacement temperature overprints magmatic foliations that are largely preserved in the inner portion of the pluton. In the Godhra Granite, mylonites and solid-state foliation developed at the northern border of the granite, at the contact with the Lunavada Group, as well as at the southern contact with the gneiss. However, at both these borders, a stretching lineation has developed with a common NW trend and this does not agree with a ballooning hypothesis. Therefore, the above evidence and arguments favour an emplacement mechanism where oblique simple shear within the gneiss was active during emplacement of the Godhra Granite.

7. Conclusions

Field, microscopic and magnetic structural studies show synmagmatic deformation and the presence of close to solidus temperatures during solid-state deformation in the Godhra Granite. Field and magnetic foliations in the granite are parallel with late stage foliation (D_3) in the gneiss. The magnetic lineation in the granite is parallel to the stretching lineation in the mylonitized margins of the granite, and also parallel to the fold axes of D_3 reclined folds. Therefore, the development of deformation fabric in the granite can be correlated with the last deformation (D_3) in the host-rock gneiss. The character of the stretching lineations and the D_3 fold axes, and the vergence of D_3 folds imply oblique simple shear. A comparison of structural data in the gneiss (present study) with the known data from surrounding Aravalli Supergroup metasedimentary rocks reveals that at a regional scale, the D_3 deformation in the gneiss, D_3 in the Lunavada Group and deformation of the Champaner Group rocks are related and synchronous events, and the emplacement of the Godhra Granite was syntectonic with them. Since the geochronological information available from the granite and Lunavada Group rocks points to a ca. 1 Ga age tectonothermal event, it is inferred that the emplacement of the Godhra Granite, deformation of the southern parts of

AMB, tectonothermal events along the CITZ and Rodinia Supercontinent assembly were related processes.

Acknowledgements

The authors are grateful to Keith Benn and an anonymous reviewer for constructive comments that enabled us to considerably improve the quality of this paper. Agnus Kontony and Carsten Wahle are thanked for helping in magnetic mineralogical studies. MAM acknowledges funding provided by the Department of Science and Technology (DST, New Delhi) to carry out research on granitoids of the southern Aravalli region under the Fast Track Proposal for Young Scientists Programme (Project No. SR/FTP/ES-23/2000). MAM's research stay at the University of Heidelberg (Germany) to perform AMS analyses was funded by the German Academic Exchange Service (DAAD, Bonn) under the Reinvitation Programme-2002.

References

Alonso Olazabal, A., Carradeco, M., Aranguren, A., 1999. Petrology, magnetic fabric and emplacement in a strike-slip regime of a zoned peraluminous granite: the Campanario–La Haba pluton, Spain. In: Castro, A., Fernàndez, C., Vigneresse, J.L. (Eds.), Understanding Granites: Integrating New and Classical Techniques Special Publications, 168. Geological Society, London.

Archanjo, C.J., Bouchez, J.L., Corsini, M., Vauchez, A., 1994. The Pombal granite pluton: magnetic fabric, emplacement and relationships with the Brasiliano strike-slip setting of NE Brazil (Paraiba State). Journal of Structural Geology 16, 323–336.

Bakker, R.J., Mamtani, M.A., 2000. Fluid inclusions as metamorphic process indicators in the southern Aravalli mountain belt (India). Contributions to Mineralogy and Petrology 139, 163–179.

Benn, K., Ham, M.N., Pignotta, G.S., Bleeker, W., 1998. Emplacement and deformation of granites during transpression: magnetic fabrics of the Archean Sparrow pluton Slave Province, Canada. Journal of Structural Geology 20, 1247–1259.

Benn, K., Roest, W.R., Rochette, P., Evans, N.G., Pignotta, G.S., 1999. Geophysical and structural signatures of syntectonic batholith construction: the South Mountain Batholith Meguma Terrane, Nova Scotia. Geophysics Journal International 136, 144–158.

Benn, K., Paterson, S.R., Lund, S.P., Pignotta, G.S., Kruse, S., 2001. Magmatic fabrics in batholiths as markers of regional strains and plate kinematics: example of the cretaceous Mt. Stuart Batholith. Physics and Chemistry of the Earth Part A—Solid Earth And Geodesy 26 (4–5), 343–354.

Berthé, D., Choukroune, P., Jegouzo, P., 1979. Orthogneiss, mylonite and non-coaxial deformation of granites: the example of the South Armorican Shear Zone. Journal of Structural Geology 1, 31–42.

Bhowmik, S.K., Dasgupta, S., 2004. Tectonometamorphic evolution of boudin-type granulites in the Central Indian Tectonic Zone and in the Aravalli Delhi mobile belt: a synthesis and future perspectives. Geological Survey of India Special Publication 84, 227–246.

Blenkinsop, T., 2000. Deformation Microstructures and Mechanisms in Minerals and Rocks. Kluwer Academic Publishers, Dordrecht.

Borradaile, G.J., 1988. Magnetic susceptibility, petrofabrics and strain. Tectonophysics 156, 1–20.

Borradaile, G.J., Alford, C., 1987. Relationship between magnetic susceptibility and strain in laboratory experiments. Tectonophysics 133, 121–135.

Borradaile, G.J., Henry, B., 1997. Tectonic applications of magnetic susceptibility and its anisotropy. Earth Science Reviews 42, 49–93.

Bouchez, J.-L., 1997. Granite is never isotropic: an introduction to AMS studies of granitic rocks. In: Bouchez, J.L., Hutton, D.W.H., Stephens, W.E. (Eds.), Granite: from Segregation of Melt to Emplacement Fabrics. Kluwer Academic Publishers, Dordrecht, pp. 95–112.

Bouchez, J.-L., Gleizes, G., Djouadi, T., Rochette, P., 1990. Microstructure and magnetic susceptibility applied to emplacement kinematics of granites: the example of the Foix pluton (French Pyrenees). Tectonophysics 184, 157–171.

Brown, M., Solar, G.S., 1998a. Granite ascent and emplacement during contractional deformation in convergent orogens. Journal of Structural Geology 20, 1365–1393.

Brown, M., Solar, G.S., 1998b. Shear-zone systems and melts: feedback relations and self-organization in orogenic belts. Journal of Structural Geology 20, 211–227.

Condie, K.C., 2001. Continental growth during formation of Rodinia at 1.35–0.9 Ga. Gondwana Research 4, 5–16.

Crawford, A.R., 1975. Rb–Sr age determination for the Mount Abu granite and related rocks of Gujarat. Journal of Geological Society of India 16, 20–28.

Cruden, A.R., Launeau, P., 1994. Structure, magnetic fabric and emplacement of the Archean Lebel Stock, SW Abitibi Greenstone Belt. Journal of Structural Geology 16, 677–691.

de Wall, H., Greiling, R.O., Sadek, M.F., 2001. Post-collisional shortening in the late Pan-African Hamisana high strain zone, SE Egypt: field and magnetic fabric evidence. Precambrian Research 107, 79–194.

Deb, M., Thorpe, R.I., Krstic, D., Corfu, F., Davis, D.W., 2001. Zircon, U–Pb and galena Pb isotope evidence for an approximate 1.0 Ga terrane constituting the western margin of the Aravalli–Delhi orogenic belt, northwestern India. Precambrian Research 108, 195–213.

Dewey, J.F., Holdsworth, R.E., Strachan, R.A., 1998. Transpression and transtension zones. In: Holdsworth, R.E., Strachan, R.A., Dewey, J.F. (Eds.), Continental Transpressional and Transtentional Tectonics Special Publication, 135. Geological Society, London, pp. 1–14.

D'Lemos, R.S., Brown, M., Strachan, R.A., 1992. Granite magma generation, ascent and emplacement within a transpressional orogen. Journal of Geological Society, London 149, 487–490.

Ferré, E., Gleizes, G., Caby, R., 2002. Obliquely convergent tectonics and granite emplacement in the Trans-Saharan belt of Eastern Nigeria—a synthesis. Precambrian Research 114, 199–219.

Fossen, H., Tikoff, B., 1998. Extended models of transpression and transtension, and application to tectonic settings. In: Holdsworth, R.E., Strachan, R.A., Dewey, J.F. (Eds.), Continental Transpressional and Transtentional Tectonics Special Publication, 135. Geological Society, London, pp. 15–33.

Gattacceca, J., Orsini, J.B., Bellot, J.P., Henry, B., Rochette, P., Rossi, P., Cherchi, G., 2004. Magnetic fabric of granitoids from Southern Corsica and Northern Sardinia and implications for Late Hercynian tectonic setting. Journal of the Geological Society 161, 277–289.

Gopalan, K., Trivedi, J.R., Merh, S.S., Patel, P.P., Patel, S.G., 1979. Rb–Sr age of Godhra and related granites, Gujarat (India). Proceedings of Indian Academy of Sciences (Earth Planetary Science) 88A, 7–17.

Gopalan, K., Macdougall, J.D., Roy, A.B., Murali, A.V., 1990. Sm–Nd evidence for 3.3 Ga old rocks in Rajasthan, northwestern India. Precambrian Research 48, 287–297.

Gopinath, K., Prasad Rao, A.D., Murty, Y.G.K., Krishnaunni, K.K., 1977. Precambrian of Baroda and Panchmahals, Gujarat. Elucidation of stratigraphy and structure. Records of Geological Survey of India 108, 60–68.

Greiling, R.O., Verma, P.K., 2001. Strike-slip tectonics and granitoid emplacement: an AMS fabric study from the Odenwald Crystalline Complex, SW Germany. Mineralogy and Petrology 72, 165–184.

Gupta, S.N., Arora, Y.K., Mathur, R.K., Iqbaluddin, Prasad, B., Sahai, T.N.,

Sharma, S.B., 1995. Geological map of the Precambrians of the Aravalli region, southern Rajasthan and northeastern Gujarat, India. Geological Survey of India Publication.

Heron, A.M. 1953. The geology of central Rajputana. Memoirs of Geological Survey of India 79.

Hrouda, F., 1993. Theoretical models of magnetic anisotropy to strain relationship revisited. Physics of the Earth and Planetary Interiors 77, 237–249.

Hrouda, F., Janak, F., 1976. The changes in shape of the magnetic susceptibility ellipsoid during progressive metamorphism and deformation. Tectonophysics 34, 135–148.

Hrouda, F., Taborska, S., Schulmann, K., Jezeck, J., Dolejs, D., 1999. Magnetic fabric and rheology of co-mingled magmas in Nasavrky Plutonic Complex (E Bohemia): implications for intrusive strain regime and emplacement mechanisms. Tectonophysics 307, 93–111.

Hutton, D.W.H., 1997. Syntectonic granites and the principle of effective stress: a general solution to the space problem? In: Bouchez, J.L., Hutton, D.W.H., Stephens, W.E (Eds.), Granite: from Segregation of Melt to Emplacement Fabrics. Kluwer Academic Publishers, Dordrecht, pp. 189–197.

Ingram, G.M., Hutton, D.W.H., 1994. The Great Tonalite Sill: emplacement into a contractional shear zone and implications for Late Cretaceous to early Eocene tectonics in southeastern Alaska and British Columbia. Geological Society of America Bulletin 106, 715–728.

Jambusaria, B.B., Merh, S.S., 1967. Deformed greywacke conglomerates of Jaban near Sivrajpur, Panchmahals district, Gujarat. Indian Minerals 8, 6–10.

Jamison, W.R., 1991. Kinematics of compressional fold development in convergent wrench terranes. Tectonophysics 190, 209–232.

Jelinek, V., 1981. Characterization of the magnetic fabrics in rocks. Tectonophysics 79, 63–67.

Jones, R.R., Holdsworth, R.E., 1998. Oblique simple shear in transpression zones. In: Holdsworth, R.E., Strachan, R.A., Dewey, J.F. (Eds.), Continental Transpressional and Transtentional Tectonics Special Publication, 135. Geological Society, London, pp. 35–40.

Kruhl, J.H., 1996. Prism- and basal-plane parallel subgrain boundaries in quartz: a microstructural geothermobarometer. Journal of Metamorphic Geology 14, 581–589.

Leblanc, D., Gleizes, G., Roux, L., Bouchez, J.L., 1996. Variscan dextral transpression in the French Pyrenees: new data from the Pic des Trois-Seigneurs granodiorite and its country rocks. Tectonophysics 261, 331–345.

Lister, G.S., Snoke, A.W., 1984. S–C mylonites. Journal of Structural Geology 6, 617–638.

Mainprice, D., Bouchez, J.-L., Blumenfeld, P., Tubiá, J.M., 1986. Dominant c-slip in naturally deformed quartz: implications for dramatic plastic softening at high temperature. Geology 14, 581–589.

Mamtani, M.A., Greiling, R.O., Karanth, R.V., Merh, S.S., 1999a. Orogenic deformation and its relationship to AMS fabric—an example from the southern margin of the Aravalli Mountain Belt, India. In: Radhakrishna, T., Piper, J.D. (Eds.), The Indian Subcontinent and Gondwana: a Palaeomagnetic and Rock Magnetic Perspective Geological Society of India Memoir, 44, pp. 9–24.

Mamtani, M.A., Karanth, R.V., Greiling, R.O., 1999b. Are crenulation cleavage zones mylonites on the microscale? Journal of Structural Geology 21, 711–718.

Mamtani, M.A., Karanth, R.V., Merh, S.S., Greiling, R.O., 2000. Tectonic evolution of the southern part of Aravalli Mountain Belt and its environs—possible causes and time constraints. Gondwana Research 3, 175–187.

Mamtani, M.A., Merh, S.S., Karanth, R.V., Greiling, R.O., 2001. Time relationship between metamorphism and deformation in the Proterozoic rocks of Lunavada region, southern Aravalli mountain belt (India)—a microstructural study. Journal of Asian Earth Sciences 19, 195–205.

Mamtani, M.A., Karmakar, B., Merh, S.S., 2002. Evidence of polyphase deformation in gneissic rocks around Devgadh Bariya: implications for evolution of Godhra Granite in the southern Aravalli region (India). Gondwana Research 5, 401–408.

McCaffrey, K.J.W., Miller, C.F., Karlstrom, K.E., 1999. Synmagmatic deformation patterns in the Old Woman Mountains, SE California. Journal of Structural Geology 21, 335–349.

McNulty, B.A., Tobisch, O.T., Cruden, A.R., Gilder, S., 2000. Multistage emplacement of the Mount Givens pluton Central Sierra Nevada batholith. Geological Society of America Bulletin 112, 119–135.

Merh, S.S., 1995. Geology of Gujarat. Geological Society of India Publication, Bangalore.

Mukherji, A., Chaudhuri, A.K., Mamtani, M.A., 2004. Regional scale strain variations in the Banded Iron Formations of Eastern India: results from anisotropy of magnetic susceptibility studies. Journal of Structural Geology 26, 2175–2189.

Naqvi, S.M., Divakar Rao, V., Narian, H., 1974. The Protocontinental growth of the Indian shield and the antiquity of its rift valleys. Precambrian Research 1, 345–398.

Neves, S.P., Araujo, A.M.B., Correia, P.B., Mariano, G., 2003. Magnetic fabrics in the Cabanas Granite (NE Brazil) Interplay between emplacement and regional fabrics in a dextral transpressive regime. Journal of Structural Geology 25, 441–453.

Pandit, M.K., Carter, L.M., Ashwal, L.D., Tucker, R.D., Torsvik, T.H., Jamtveit, B., Bhushan, S.K., 2003. Age, petrogenesis and significance of 1 Ga granitoids and related rocks from the Sendra area, Aravalli craton, NW India. Journal of Asian Earth Sciences 22, 363–381.

Passchier, C.W., Trouw, R.A.J., 1996. Microtectonics. Springer, Berlin.

Paterson, S.R., Vernon, R.H., Tobisch, O.T., 1989. A review of criteria for the identification of magmatic and tectonic foliations in granitoids. Journal of Structural Geology 11, 349–363.

Pignotta, G.S., Benn, K., 1999. Magnetic fabric of the Barrington Passage pluton Meguma Terrane, Nova Scotia: a two-stage fabric history of syntectonic emplacement. Tectonophysics 307, 75–92.

Pressley, R.A., Brown, M., 1999. The Phillips pluton Maine, USA: evidence of heterogeneous crustal sources and implications for granite ascent and emplacement mechanisms in convergent orogens. Lithos 46, 335–366.

Rochette, P., 1987. Magnetic susceptibility of the rock matrix related to magnetic fabric studies. Journal of Structural Geology 9, 1015–1020.

Rochette, P., Jackson, M., Aubourg, C., 1992. Rock magnetism and the interpretation of anisotropy of magnetic susceptibility. Reviews in Geophysics 30, 209–226.

Rochette, P., Scaillet, B., Guillot, S., Lefort, P., Pecher, A., 1994. Magnetic-properties of the high Himalayan leucogranites—structural implications. Earth And Planetary Science Letters 126, 217–234.

Roy, A.B., 1988. Stratigraphic and tectonic framework of the Aravalli mountain range. In: Roy, A.B. (Ed.), Precambrian of the Aravalli mountain, Rajasthan, India Geological Society of India, Memoir, 7, pp. 3–31.

Roy, A.B., Kröner, A., 1996. Single zircon evaporation ages constraining the growth of the Archean Aravalli craton, northwestern Indian shield. Geological Magazine 133, 333–342.

Saint-Blanquat, M., Tikoff, B., 1997. Development of magmatic to solid-state fabrics during syntectonic emplacement of the Mono Creek granite, Sierra Nevada Batholith, California. In: Bouchez, J.L., Hutton, D.W.H., Stephens, W.E. (Eds.), Granite: From Segregation of Melt to Emplacement Fabrics. Kluwer Academic Publishers, Dordrecht, pp. 231–252.

Saint-Blanquat, M., Tikoff, B., Teyssier, C., Vigneresse, J.L., 1998. Transpressional kinematics and magmatic arcs. In: Holdsworth, R.E., Strachan, R.A., Dewey, J.F. (Eds.), Continental Transpressional and Transtentional Tectonics Special Publication, 135. Geological Society, London, pp. 327–340.

Scaillet, B., Pecher, A., Rochette, P., Champenois, M., 1995. The Gangotri Granite (Garhwal Himalaya)—Laccolithic emplacement in an extending collisional belt. Journal of Geophysical Research-Solid Earth 100, 585–607.

Siegesmund, S., Becker, J.K., 2000. Emplacement of Ardara pluton (Ireland): new constraints from magnetic fabrics, rock fabrics and age dating. International Journal of Earth Sciences 98, 307–327.

Simpson, C., 1985. Deformation of granitic rocks across the brittle–ductile transition. Journal of Structural Geology 7, 503–511.

Simpson, C., Wintsch, R.P., 1989. Evidence for deformation induced K-feldspar replacement by myrmekite. Journal of Metamorphic Geology 7, 261–275.

Solar, G.S., Pressley, R.A., Brown, M., Tucker, R.D., 1998. Granite ascent in convergent orogenic belts: testing a model. Geology 26, 711–714.

Tarling, D.H., Hrouda, F., 1993. The Magnetic Anisotropy of Rocks. Chapman and Hall, London.

Tobisch, O.T., Collerson, K.D., Bhattacharyya, T., Mukhopadhyay, D., 1994. Structural relationship and Sr–Nd systematics of polymetamorphic granitic gneisses and granitic rocks from central Rajasthan India: implications for the evolution of the Aravalli craton. Precambrian Research 65, 319–339.

Tomezzoli, R.N., MaCdonald, W.D., Tickyj, H., 2003. Composite magnetic fabrics and S–C structure in granite gneiss of Cerro de lo Viejos La Pampas province, Argentina. Journal of Structural Geology 25, 159–169.

Verma, P.K., Greiling, R.O., 1995. Tectonic evolution of the Aravalli orogen (NW India): an inverted Proterozoic rift basin? Geologische Rundschau 84, 683–696.

Vernon, R.H., 2000. Review of microstructural evidence of magmatic and solid-state flow. Electronic Geosciences 5, 2.

Vigneresse, J.L., Clemens, J.D., 2000. Granitic magma ascent and emplacement: neither diapirism nor neutral buoyancy. In: Vendeville, B., Mart, Y., Vigneresse, J.L. (Eds.), Salt, Shale and Igneous Diapirs in and around Europe Special Publication, 174. Geological Society, London, pp. 1–19.

Vigneresse, J.L., Tikoff, B., 1999. Strain partitioning during partial melting and crystallizing felsic magmas. Tectonophysics 312, 117–132.

Volpe, A.M., Macdougall, J.D., 1990. Geochemistry and isotopic characterization of mafic (Phulad Ophiolite) and related rocks in Delhi Supergroup Rajasthan, India: implication of rifting in Proterozoic. Precambrian Research 48, 167–191.

Wiedenbeck, M., Goswami, J.N., Roy, A.B., 1994. Stabilization of the Aravalli craton of northwestern India at 2.5 Ga: an ion microprobe study. Chemical Geology 129, 325–340.

Yedekar, D.B., Jain, S.C., Nair, K.K.K., Dutta, K.K., 1990. The central Indian collision suture. Geological Survey of India Special Publication 28, 1–43.

Yoshida, M., Divi, R.S., Santosh, M., 2001. Precambrian central India and its role in the Gondwanaland–Rodinia context. Gondwana Research 4, 208–211.